Estimation of Air-Pressure Drop in Inclined Penstocks during an Emergency Closure of Intake Gates

Michel-Olivier Huard

A Thesis

in

The Department

of

Building, Civil and Environmental Engineering

Presented in Partial Fulfilment of the Requirements

For the Degree of

Master of Applied Science

Concordia University

Montreal, Quebec, Canada

September 2014

CONCORDIA UNIVERSITY
School of Graduate Studies

This is to certify that the thesis prepared

By: Michel-Olivier Huard

Entitled: Estimation of Air-Pressure Drop in Inclined Penstocks during an Emergency Closure of Intake Gates

and submitted in partial fulfillment of the requirements for the degree of

Master of Applied Science (Civil Engineering)

complies with the regulations of the University and meets the accepted standards with respect to originality and quality.

Signed by the final examining committee:

_____ Chair

_____ Examiner

_____ Examiner

_____ Supervisor

Approved by _____
Chair of Department or Graduate Program Director

_____
Dean of Faculty

Date _____

ABSTRACT

Estimation of Air Pressure Drop in Inclined Penstocks during an Emergency Closure of Intake Gates

Michel-Olivier Huard

Concordia University, 2014

Hydroelectric power is an important source of energy. This is particularly true for Quebec and some other provinces in Canada. In the event of a combination of power trip and wicket gate blockage, as an emergency response, it is necessary to close the intake gates in order to stop water flow through the penstock to the unit. Such emergency closure can cause air pressure inside the penstock chamber to drop so significantly that the safety risks to the power station structures and facilities become unacceptable. The purpose of this study is to develop analysis methods for the assessment of air pressure drop in emergency closure. The scope of this research work covers the determination of the following time-dependent quantities: water discharge beneath a sluice gate, dry air flow through air vents leading to the penstock chamber, amount of air entrained by turbulent water motions through the penstock, and the resultant changes of air pressure in the penstock chamber. The analyses are based on the energy principle and take into account a large number of variables including the upstream and downstream water levels, the geometry of the hydraulic passage, the time rate of gate closing, and features of downstream control structures. The analysis methods are applied to two cases of emergency closure of power generating stations in Quebec. The results of calculated air demand and pressure drop are in good comparison with field measurements. Emergency closure is shown to produce two significant

impacts on penstocks and air vents: 1) intensified water jet in the first half of the time period it takes to close the gate; and 2) pressure drop in the last one third of the time period. Air entrainment by high-velocity flowing water is an important cause of pressure drop in emergency closure, and can be modeled using hydraulic jump entrainment equations. The values of air pressure drop calculated for the Isle-Maligne and La Tuque stations are below one third of the standard atmospheric pressure. However, there are significant air pressure fluctuations. This study has contributed to the development of quantitative framework and calculation procedures that can easily be extended for applications to other sites. The development is of engineering relevance to upgrade of existing air vents and the design of new air vents and to safe operations of emergency closure.

ACKNOWLEDGEMENTS

I would like to express my gratitude to my supervisor Dr. Samuel Li for the useful comments, remarks and engagement through the learning process of this Master's thesis. Furthermore, I would like to thank Yannick Bossé for inspiring me to work on the topic as well as for his great support along the way. Also, I would like to thank AECOM (formerly RSW) and Rio-Tinto Alcan for providing me with the precious field measurements and drawings. I would like to thank my wife Isabelle, who has supported me throughout the entire process.

TABLE OF CONTENTS

LIST OF TABLES

LIST OF FIGURES

LIST OF NOMENCLATURE

A	Equivalent net flow area (m^2)
B	Average flow width at gate section (m)
BL	Blade level (m)
C_d	Discharge coefficient
C_c	Contraction coefficient
D	Hydraulic diameter (m)
f	Friction factor
F	Froude number
g	Acceleration of gravity (m/s^2)
h	Head (m)
h_f	Major head loss (m)
h_L	Head loss (m)
h_m	Minor head loss (m)
k	Minor loss coefficient
L	Length (m)
m	mass of air (kg)
P	Pressure (Pa)
P_a	Air pressure (Pa)
Q	Water flow rate through the gate (m^3/s)
Q_o	Air volumetric flow fraction in water (m^3/s)

Q_{out}	Water flow through the turbine (m^3/s)
Q_{11}	Turbine flow parameter
q	Discharge per unit width of channel (m^2/s)
R_2	Reynolds Number
s	Submergence ratio
SL	Gate sill level (m)
Δt	Simulation time step duration (s)
V	Water volume in the penstock (m^3)
V_a	Air volume in the penstock (m^3)
v	Cross-sectional average velocity (m/s)
w	gate opening (m)
WL	Upstream water level (m)
y	Water depth (m)
Z	Turbine flow power coefficient
z	Elevation (m)
β	Air to water volumetric ratio
ε	Absolute roughness (m)
γ	Specific weight (N/m^3)
ρ_a	Air density ($kg/m3$)

1. INTRODUCTION

1.1 Motivation of this Study

Hydroelectric power is a vital source of energy for many regions around the world. This is particularly the case for Quebec (Close to 96% of its electricity is produced through hydropower) as well as other provinces in Canada. In the 21st century, rivers in Quebec that are the most economical for power exploitations have already undergone their great transformation (Figure 1-1). Unexploited rivers remain so either because the sites are too far from large consuming centers or the flow rate and/or the head are too low, and thus do not offer good opportunities or because the construction of dams on the watercourse will have real or perceived excessive negative social and environmental impact.

A great number of hydroelectric generating stations in Quebec were built during the first quarter of the 20th century and almost all of them still operate with a major part of the original components and equipment. In the event of a failure of turbine-generator unit, it will be necessary to close the upstream intake gates in order to stop water flow through the penstock to the turbine-generator unit as an emergency response (Figure 1-2). How high will the safety risks be to the aging station structural and mechanical components caused by air pressure drop in the penstock chamber during an emergency closure?

In fact, some generating stations need an urgent rehabilitation. Examples include the rehabilitation of the intake, spillway and gravity dam at La Tuque generating station (Figure 1-2a) to ensure long-term facility safety. This generating station (owned by Hydro-Quebec) is located at (47º26'39"N, 72º47'58"W). It was commissioned in 1940-1955, with a capacity of 294

megawatts. It is a run-of-river type of station (Figure 1-2a), with a head of 34.75 m. La Tuque generating station will be used to demonstrate the applicability of analysis methods to be presented in this thesis. For the same purpose, the Isle-Maligne generating station (owned by Rio Tin Alcan) built in 1926 will also be used. This generating station is located at (48º34'37"N, 71º38'05"W); it has a capacity of 402 megawatts.

Figure 1-1 Locations of hydroelectric generating stations in Quebec (from http://www.unites.uqam.ca/hypera/index.html , accessed on September 16, 2014)

(a)

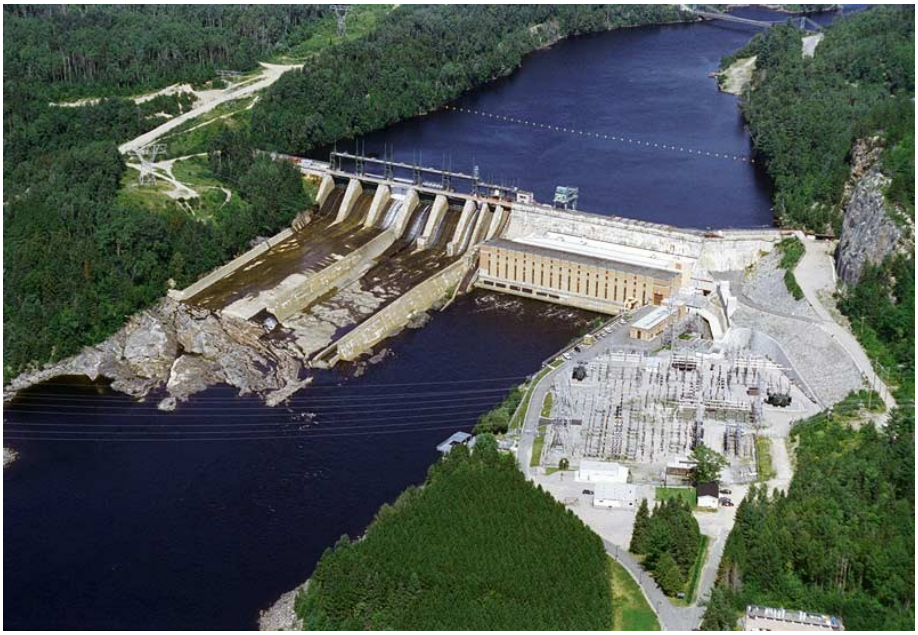

(b)

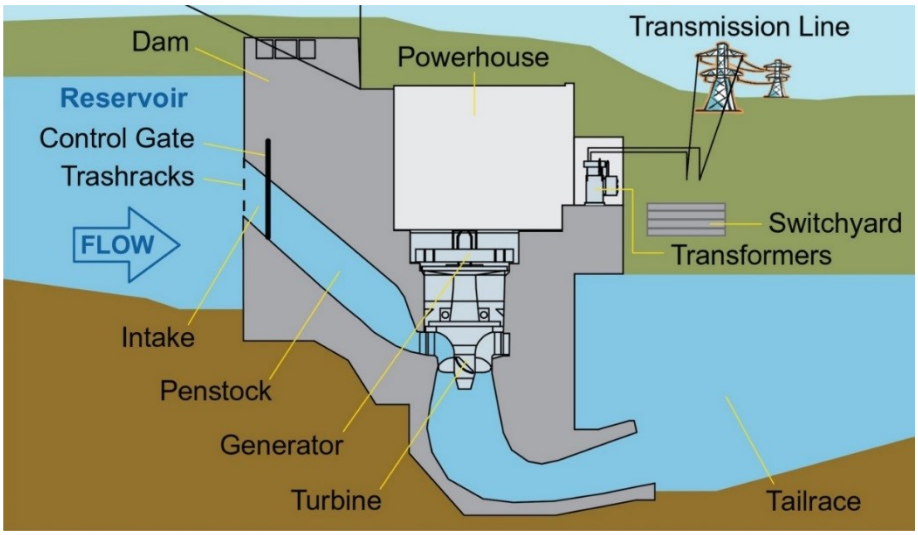

Figure 1-2 Hydroelectric generating stations: (a) The spillway and intake at La Tuque generating station on the St. Maurice River, between Trois-Rivières and Chambord, Quebec (adopted from Hydro-Quebec); (b) a vertical cross section of a typical hydroelectric generating station, showing an intake gate, a penstock, a turbine-generator unit, and a tailrace (adopted from Nalcor Energy).

Until recently it has been generally believed that it is more economical to exploit new river sites than to improve the performance of existing generating stations. This era appears to be taking a new turn. For a given penstock diameter (Figure 1-2), possible ways to improve the performance include: (1) designing and building more efficient turbine-generators; (2) increasing water flow; (3) optimizing operations (by means of water flow control), which is particularly advantageous for stations with a large upstream reservoir. The reason is that they can increase the proportion of electricity generated during peak hours with the same annual volume of water. Electricity sold in peak hours can be worth many times the price of that sold off-peak, giving motivation to produce more within the peak hour period. The question arises as to what will be the implications of changing flow rate to air vents (Figure 1-2).

The quest for answers to the important safety questions raised above has motivated this study. In fact, from the perspective of hydraulic engineering, the next element to assess for a turbine replacement project after the turbine itself is the air vents system. Air vents are used to provide air supply to the penstock. They are generally solicited at their maximum during an emergency closure and must be tailored to such events.

1.2 Statement of the Problem

An emergency closure is a mean of interrupting the water flow through a turbine-generator unit. This is accomplished by lowering the intake gate (Figure 1-2), as opposed to using wicket gates to control and stop the flow in regular closures. The wicket gates are located around the turbine, at the bottom of the water column; closing them will produce a positive pressure in the upstream column. On the contrary, the head gates are located at the intake of the water passage, at the top

of the water column. Flow interruption by the intake gate is likely to produce a negative pressure in the underling column. Too great a vacuum within the penstock may cause the head gate itself to break, the separation of concrete patches within the penstock which could destroy the turbine, or even the collapse of the generator's floor located above the penstock. A broken head gate during emergency closure would be particularly problematic with the wicket gates being locked in fully or partially open position. It would then be very difficult, if not impossible, to cut the water flow through the turbine.

It is important for owners of hydroelectric generating stations to gain accurate data of pressure distribution associated with this rare but important event and to understand any sensitive elements that could lead to a catastrophe. Emergency closures have never been tested before on prototypes for specific reasons: It is difficult to monitor the conditions and outcomes are unknown; there has never been a manifestation of desire before today to know if a penstock could withstand or not an emergency closure; every owner relies on the accuracy of the original design, not wanting to take the chance of testing it.

It is to the owners' interest to increase turbine flow. However, are existing air vents adequate to maintain safe air pressure in the penstock? What will the minimum air pressure be? No precise methods for analyzing the problem have been reported in the literature.

1.3 Objectives of this Research Work

The current practice with regard to air supply to penstocks is that engineers use a rule of thumb to determine the size of air vents, often on the basis of the maximum rate of water flow for turbine-generator operations. This is an approximation that may be inconsistent with

fundamental fluid mechanics principles and, to a large extent, is inaccurate for the situation of intake gate closures. Although the maximum flow rate will have a great impact on vacuum pressure, there are uncertainties in the result when other factors are excluded from the estimation.

The objectives of this study are

1) to improve our understanding of the process of unsteady flow beneath an intake gate whose opening is changing;
2) to reveal the effect of turbulent water motions in a penstock on entraining air;
3) to develop the procedures for determining changing air pressure with the use of fluid mechanics principles.

1.4 Scope of the Work

This research work involves theoretical formation of water and air flow in the hydraulic passages of a penstock, application to two selected field sites, compilation of field measurements, and comparison of the analytical results to the field measurements. The remaining part of this thesis is organized as follows:

The next section will give the highlight of contributions from this research work.

Chapter Two will provide a critical review of the pertinent literature. The review covers publications on discharge passing through an underflow gate, air flow in closed conduits, hydraulic jumps, and air entrainment by turbulent water flow.

Chapter Three will describe the theory for quantitative analyses of unsteady flow of water and air based on the energy concept as well as the procedures for the assessment of the air pressure field.

Chapter Four will present and discuss the analytical results of water discharge, air demand, net air mass flow and resultant air pressure changes, along with comparison with field measurements.

Chapter Five will draw conclusions from this research work and suggest extensions for future research.

1.5 Highlight of Research Contributions

Prior investigations of underflow gates, flow in air vents and air entrainment by turbulent water motions have led to the establishment of theoretical / semi-theoretical formulae, with impressive practical application. However, the investigations suffer a number of significant limitations: They focused on steady conditions. They dealt with the processes of water flow and air flow separately. Contributions from this research are highlighted next:

1) This study has added the consideration of time-dependence and between-process interaction when dealing with the problem of air pressure drop in penstocks. Also, this study has demonstrated applications to real-world generating stations at the field scale, without uncertainties associated with artificial scale effects at the laboratory scale.
2) Field measurements of air flow and pressure were collected at La Tuque generating station in 2006 and at Isle Maligne generating station in late 2013. The selection of hydraulic measuring instruments (with the exception of the Propeller-type current meters; see appendix B – instrument No 28 to 43) and positioning for the later measuring campaign were done by the author The performed measurements, along with data of geometry, operating water levels and flow rates are valuable for theory and model

validations. The author also performed all raw data processing presented in this study.

2. REVIEW OF THE LITERATURE

2.1 Sluice Gates

Gates are used to control the flow typically in open channels. An example of a vertical gate structure and gate lift is shown in Figure 2-1a. A sketch of flow passing under a vertical gate in a horizontal channel is shown in Figure 2-1b. Vertical gates are referred to as vertical lift gates, sluice gates or vertical sluice gates. The sluice gates are raised and lowered by supporting vertical guides with roller wheels (Figures 2-2a-b). Depending on the blade shape, fast running water under the gate can either exert down pull or up force on the gate.

(a)

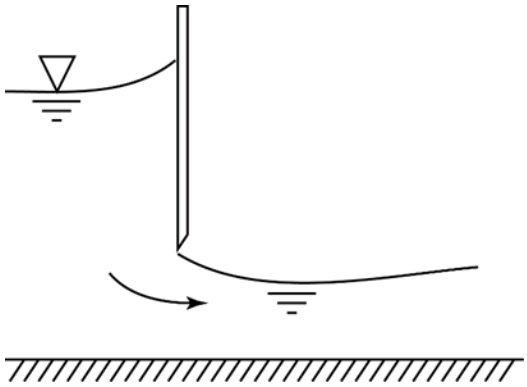

(b)

Figure 2-1 a) A photo of a vertical gate structure designed for underflow operation (from http://ceephotos.karcor.com/tag/sluice-gate/, accessed on September 1, 2014); (b) A vertical section of a sluice gate in a horizontal channel, showing flow passing beneath the gate.

(a)

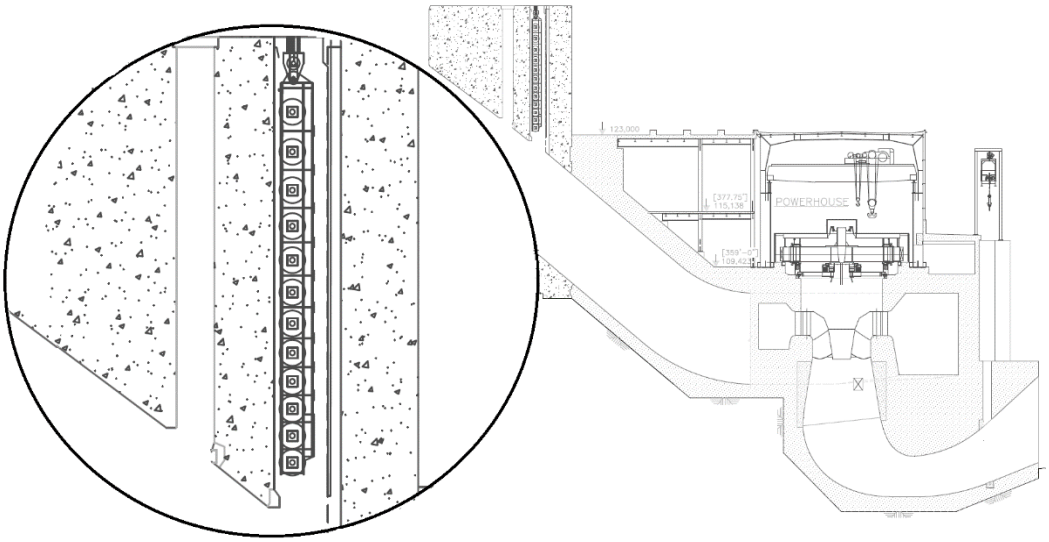

(b)

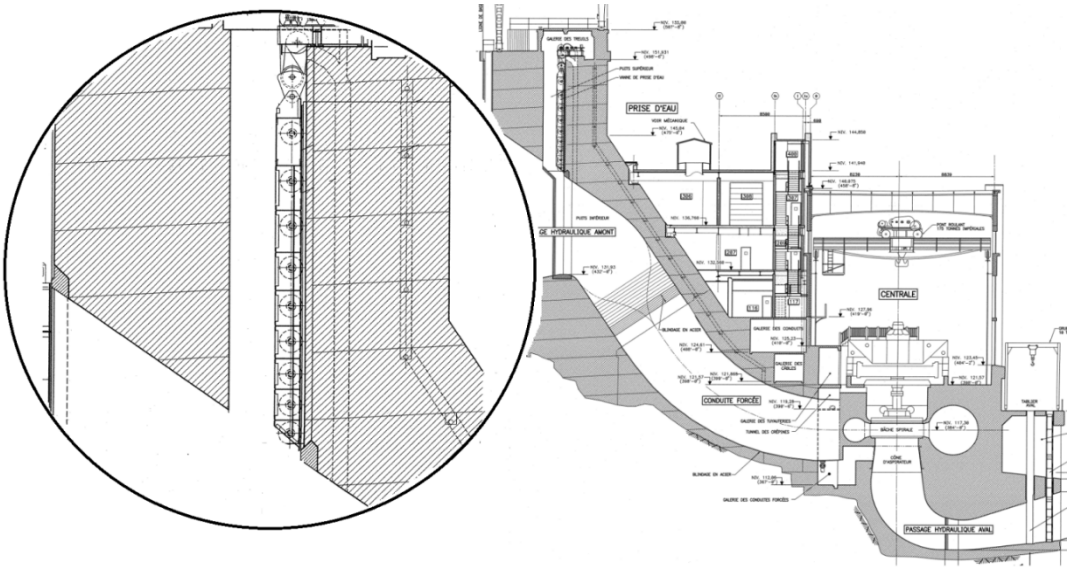

Figure 2-2 Hydroelectric generating stations: (a) The Harmon generating station with a Stoney gate of upstream seal configuration; (b) the La Tuque generating station with a Stoney gate of downstream seal configuration (Modified from a drawing prepared by AECOM for Ontario Power Generation).

Intake gates for hydropower applications operate in the same principle as the sluice gates

described in the preceding section. Vertical-lift intake gates can be of the upstream or downstream sealing type, as illustrated in Figures 2-2a-b. A close-up view of the gate wells is shown in the circles. In Figure 2-2a, the gate well also serves as an air vent, whereas in Figure 2-2b, there is a separate air vent. For detailed structural design guidelines, refer to Sagar (1995) and Sehgal (1996).

2.2 Flow Passing under Underflow Gates

From the hydraulics perspective, it is important to be able to determine discharge, Q, passing through a sluice gate. Under free-flow discharge condition, the outflow beneath the gate is a wall-bounded (or bottom-bounded) jet, driven by the difference in pressure between the upstream and downstream sides of the gate. The outflow streamlines contract downstream of the gate until the flow reaches the minimum depth at a cross section known as the vena contracta. As an approximation, the jet flow is considered to be one-dimensional, in the longitudinal direction (Figure 2-1b). In order to determine Q, the energy equation can be applied between a cross section well upstream of the gate and the vena contracta, producing an expression for Q as a function of the depth of water at the upstream cross section (Henderson, 1966, p. 202–203).

This expression contains the discharge coefficient, C_d. This coefficient is introduced to account for deviations from the orifice-flow assumption. C_d depends on the amount of energy losses between the two cross sections and the amount of flow contraction. C_d is a key parameter and has attracted substantial research attention. The classic work by Henry (1950) produced widely used experimental values of C_d (Figure 2-3). Henry's (1950) work is well-referenced. According to Swamee (1992), the experimental values of C_d are the most extensive and reliable.

Swamee (1992) obtained high-accuracy discharge coefficient equations in consistency with the experimental values.

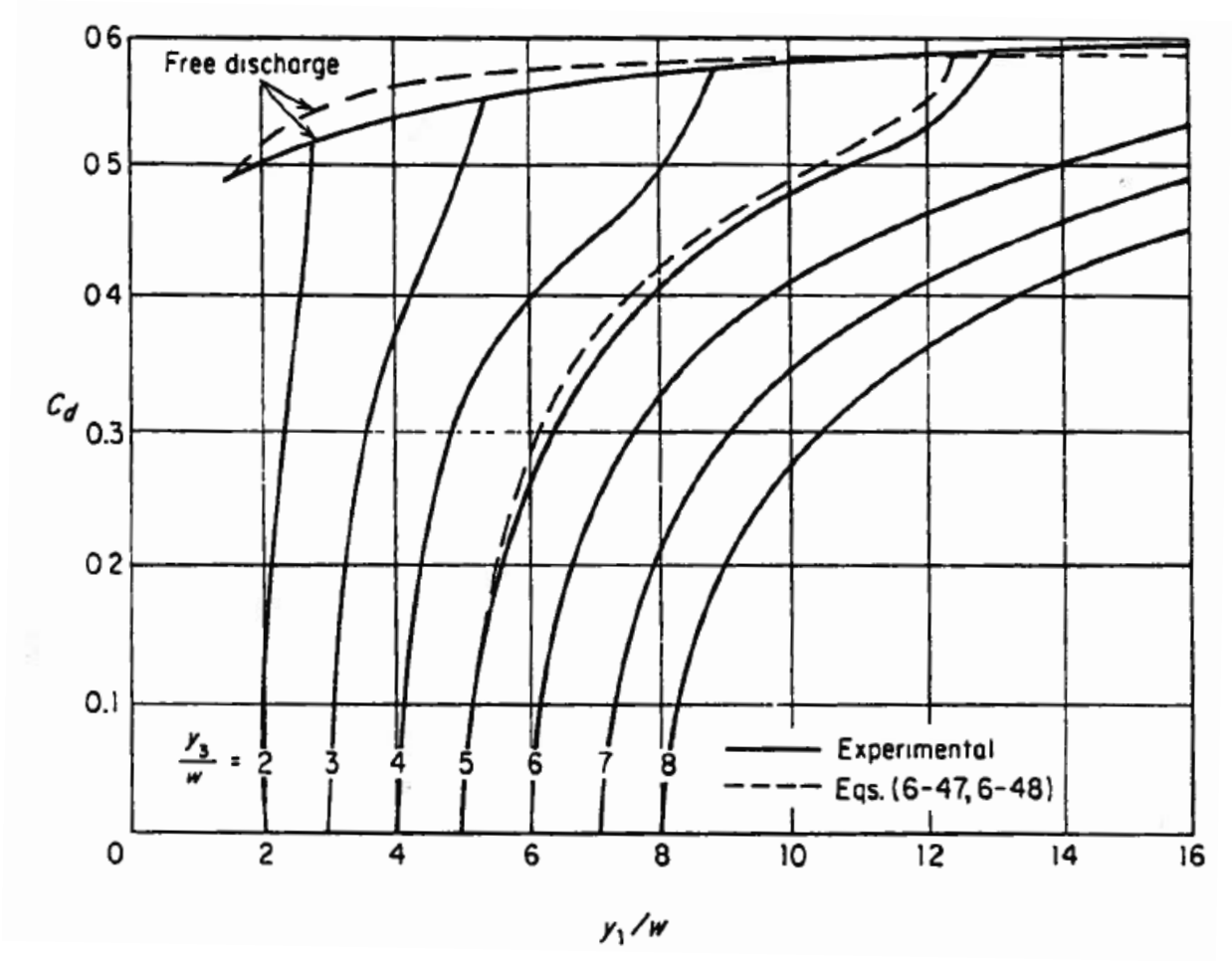

Figure 2-3 The discharge coefficient C_d of a vertical sluice gate for free and submerged flows, as a function of the upstream depth of water y_1 relative to the gate opening w, and tail-water depth (Henry, 1950)

The flow contraction is measured by two ratios: the ratio of the depth of flow at the vena contracta to the gate opening (or the contraction coefficient C_c) and the ratio of the gate opening

to the upstream depth of water. For sharp-edged vertical sluice gates, some classic experimental studies suggested values of C_c as 0.60 (Henry 1950) and 0.61 (Henderson 1966), meaning that the depth of flow at the vena contracta is 0.60 to 0.61 times the gate opening. Rajaratnam and Subramanya (1967) reported experimental results of C_c in the range of 0.58 to 0.63. Chadwick and Morfett (1993) obtained results of C_c in consistency with the earlier finding of Henderson (1966). The recent experimental results of Lin et al. (2002) gave a narrower range of Cc values (0.59 to 0.61) in comparison to the range reported in Rajaratnam and Subramanya (1967).

If the discharge beneath the gate is supercritical and the tail-water depth downstream of the gate is larger than the conjugate depth of the vena contracta, the outflow will be submerged. The problem of submerged outflow can be analyzed by combining the energy equation and momentum equation, assuming that all the energy head losses occur in the flow downstream of the gate (Chin 2012, p. 183). The approach of combining the energy-momentum equations proves to be sound; this approach has produced results in a good agreement with field data (Lozano et al. 2009)

The results of Henry (1950) covered the situation of submerged outflow (Figure 2-3). Rajaratnam and Subramanya (1967) carried out an experimental investigation of flow immediately downstream of a submerged sluice gate. A main finding is that the depth of wall-bounded jet flow at the vena contracta is 0.61 times the gate opening and the vena contracta occurs at a distance of about 1.15 times the gate opening from the gate opening.

Cassan and Belaud (2011) conducted an experimental and numerical study of flow under sluice gates. Their work focused on the condition of a large gate opening and submerged sluice gate: the ratio of the gate opening to the depth of flow at the upstream face of the gate was

greater than 0.5. The submergence ratio of the tail-water depth downstream of the vena contracta to the depth of flow on the upstream side well upstream of the stagnation zone is larger than 0.5. The authors concluded that the contraction coefficient C_c largely increases with gate opening, as opposed to being constant as $C_c = 0.61$. The conditions considered in the study typically do not apply to flow past a sluice gate into a penstock.

Habibzadeh et al. (2011) investigated the role of energy loss on discharge characteristics of sluice gates. They derived equations for the discharge coefficient under both free and submerged conditions. For free flow, values of C_d are related to the contraction coefficient, the ratio of the depth of flow upstream of the gate to the depth of the contracted jet flow downstream of the gate, and the energy loss factor. For submerged flow, C_d is related to the ratio of the depth of flow upstream of the gate to the tail-water depth as an additional parameter.

For submerged flow, energy correction is necessary for determining accurate discharges. Clemmens et al. (2003) proposed an energy correction model. Their model is based on data collected from a relatively small range of flow conditions, comprising four flow rates at a single gate position, with varying upstream and downstream depths. Clemmens et al. (2003) speculated that the energy correction relationship might vary as a function of the relative gate opening, which could not be verified from their limited data.

Wahl (2004) provided a review of the development in determining flow discharge in irrigation channels, giving a particular discussion on improving the accuracy through energy correction. The author analyzed a data set collected in the late 1970's and early 1980's, and suggested that the relative gate opening was an important parameter affecting the relationship between the relative energy correction and the relative submergence. The analysis led to an

energy correction equation, which improves the accuracy of calibrations in the transition zone. However, there remain unanswered questions related to energy correction.

2.3 Duct Flow (Air Vent Systems)

For many practical flow situations, one needs to know only air flow deliverable in ducts rather than the detailed distribution of flow velocity at the duct cross section. In a circular duct, the volumetric flow rate may be determined by dividing the cross section into three or four concentric equal areas, measuring the local velocities in each of the areas, and calculating the average of six velocity readings taken at 60º intervals round this annulus, as illustrated in Douglas et al. (2005, p. 182). This basic technique is essentially area-weighted averaging. Velocity readings may be obtained from e.g. a grid of Pitot tubes mounted across the air flow. The basic technique may also be applied to rectangular ducts, in which case, the duct cross section should be divided into at least 25 zones.

The Darcy equation can be used to calculate pressure loss due to friction (termed the major loss) in duct flow. This equation is valid for fully developed, steady state and incompressible flow. Use of the equation requires an empirical friction factor. Values of this friction factor depend on the roughness of the duct relative to the duct diameter and the Reynolds number. Values of the friction factor may be obtained from the Moody chart (Moody 1944) or from the Colebrook-White equation (Colebrook 1939).

The Darcy equation and the Colebrook-White equation can be combined to yield a relationship linking the flow rate to the conduit diameter and pressure loss per unit length. For a given flow rate, the pressure loss per unit length in circular ducts is known to increase with

decreasing duct diameter in a fifth-power relationship. One can retain the same flow velocity as flow rate increases by increasing the duct diameter. These results have direct application to duct design. Other practical applications include linking delivered flow of air to the overall cost in terms of the pressure loss.

Air flow in real-world duct systems is almost always required to pass through a variety of fittings, bends, enlargements, contractions, inlets, exits and so on. As a result, minor losses of pressure are encountered, in addition to the main loss due to friction. The additional minor losses are mainly due to flow separation triggered by the geometric features mentioned above. An example of pressure drop due to separation of flow in bends is given in Crawford et al. (2007).

One way to represent such separation losses is to use the equivalent length approach. The fitting equivalent length is added to the length of the duct to allow the overall pressure loss to be calculated using the convenient Moody chart. For example, for a 90º elbow, add an equivalent length of 30 times the duct diameter (Crane Co. 1982). Alternatively, since the concept of separation loss depends on flow kinetic energy, separation losses may be expressed as a pressure term $K_s \frac{1}{2}\rho_\circ v_a^2$, where K_s is the loss coefficient, $\rho_\circ$ is the density of air, and v_a is the velocity of air flow. Representative values of K_s for typical fittings and geometric features can be found from standard texts. For example, for inlets, K_s can be taken as 0.5.

2.4 The Hydraulic Jump and Air Entrainment

The hydraulic jump refers to a feature through which the flow transfers abruptly from the supercritical to the subcritical condition. The subcritical condition is produced by downstream

control. The depths of flow before and after the jump are said to be conjugate. The strength and characteristics of the jump depend on the Froude number of the supercritical flow (Chow, 1959, p. 395). The hydraulic jump is characterized by violent turbulence and substantial energy loss. Also, it is characterized by air entrainment (Chanson 2007). This is mainly due to boundary layer growth from the channel bed (Henderson 1966, p. 184). The concentration of entrained air in the flowing water is defined as the volumetric ratio of air to the total of air plus water. The concentration can be measured using some optic devices (Tian et al. 2010). However, reliable field data of entrained air concentration in water flow are very sparse.

In the literature, the terms air entrainment, air bubble entrainment and self-aeration are used interchangeably to refer to the exchange of air between the atmosphere and flowing water. There is a distinction between singular aeration and interface aeration: Singular aeration refers to entrainment of air bubbles localised at a flow discontinuity (Chanson 2008); air bubbles are entrained locally at the intersection of the impinging water jet with the receiving body of water; the impingement perimeter is a source of both vorticity and air bubbles. Aeration in a vertical plunging jet (Sene 1988; Smit 2007) is an example of singular aeration. Interfacial aeration means continuous entrainment of air bubbles along an air-water free-surface usually parallel to the flow direction. This can occur in such flows as spillway chute flow (Chanson 1991) and high-velocity water jet discharging into air.

In fact, the phenomenon of air entrainment occurs frequently in many hydraulic flow problems, but the mechanism of air entrainment is not yet fully understood. This is in spite of substantial research efforts made in the past. In Chanson (1996), air bubble entrainment is defined as the entrapment of air bubbles and pockets that are advected within the turbulent flow.

Chanson (2008) used the term air bubble broadly to describe a volume of air surrounded continuously or not by some liquid and encompassed within some air-water interface(s). The resulting air-water mixture consists of both air packets within water and water droplets surrounded by air, and the flow structure may be quite complicated.

Indeed, the problem of air entrainment is complicated; simple scaling arguments can give predictions of air entrainment rate over 4 orders of magnitude in the dimensionless jet speed (Lorenceau et al. 2004). In a review paper, Chanson (2009) raised concerns about the extrapolation of laboratory results to large size prototype structures using a Froude number similitude; the laboratory Reynolds numbers are typically much smaller than those in the corresponding prototype flows, which remains an unresolved issue.

From flume experiments, Gualtieri and Chanson (2007) measured the vertical distributions of void fraction and air-bubble count rate. The experimental conditions covered inflow Froude numbers in the range of 5.2 to 14.3. Their observations showed occurrences of rapid detrainment near the jump toe and a structured air diffusion layer over longer distances. By comparing their measurements with previous measurements made generally at lower Froude numbers, Gualtieri and Chanson (2007) suggested that at a fixed distance from the jump toe, the maximum void fraction increased with increasing the inflow Froude number. Their measurements included the vertical locations of the maximum void fraction and bubble count rate. Their work contributed to the derivation of an empirical correlation between the upper boundary of the air diffusion layer and the distance from the impingement point. The key finding was that the Froude number is an important parameter in air entrainment.

Chanson and Gualtieri (2008) made measurements of distributed void fraction from two experiment channels. Between the two channels, the experiments used identical inflow Froude numbers and relative channel widths. The geometric scaling ratio was 2:1. The measurements showed the presence of an advection/diffusion shear layer. The measured void fraction distributions appear to follow an analytical solution of the diffusion equation for air bubbles. There are some scale effects in the smaller channel, as seen in the measurements of void fraction and bubble count rate. The measured void fraction distributions implied relatively greater detrainment at low Reynolds numbers, yielding less overall aeration of the jump roller. Dimensionless bubble count rates were significantly lower in the smaller channel especially in the mixing layer. The study by Chanson and Gualtieri (2008) documented well that artificial scale effects can be very problematic, giving errors in determining air entrainment in the hydraulic jump.

2.5 Air Pressure in Penstocks

Low air pressures form during an emergency closure of the intake gates as water in the penstock drains through turbine-generator units. This problem can have serious consequences. For many decades, researchers (e.g. Falvey 1968; Borodina 1969; Sharma 1976) have tried to determine the time-magnitude relationships of reduced pressures inside the structure and to properly size air vent systems. The dimensions of air vents certainly affect the reduced pressure. Adequate supply of air is of paramount importance. This is also true for bottom outlets for larger dam structures (Speerli and Hager 2000). A summary of findings about air vent systems for the outlets can be found in Falvey (1980). At a high head gate, the condition can be such that the

discharge passes under the gate as well as over the top of the gate; Naudascher et al. (1986) carried out a one-dimensional analysis of the discharge under such condition.

In a classic paper about air entrainment by the hydraulic jump, Kalinske and Robertson (1943) proposed that the relationship $\beta = K(F - 1)^{1.4}$ where β is the ratio of the entrained air volumetric flow rate to water flow rate, K is a coefficient, and F is the Froude number. The Froude number was evaluated at the toe of the jump. On the basis of an experimental study, Sharma (1976) suggested that air demand in a conduit flow with the free hydraulic jump should be a function of both the entraining capacity of the jump and the carrying capacity of the flow. The carrying capacity appears to be related to the conduit slope. There is not a linear relationship between head and maximum air entrainment ratio. Sharma (1976) introduced modifications to the relationship proposed by Kalinske and Robertson (1943); the reason was that the Froude number was evaluated at the vena contracta. It is worth noting that Sharma's (1976) experiments excluded the effect of downstream pressure and were limited to steady flow conditions.

Aydin (2002) carried out a physical and numerical modelling study of air pressure drop and subsequent air demand. The results suggested a significant correlation between the numerical model and the small scale physical model. The numerical model did not account for air entrainment. It appears that air entrainment was not observed in the physical model. Therefore, there are uncertainties about how well the modelling results reflect reality. Field measurements from La Tuque hydroelectric generating station (Figures 1-1 and 2-2b) show significant air entrainment during emergency closures. Arguably, air entrainment at the field scale (real-world structures) cannot be ignored in pressure drop analyses. Thus, the physical model of a penstock undergoing an emergency closure, reported in Aydin (2002), is probably not adequate for the

validation of numerical models of total air demand. According to Borodina (1969), the quantity of entrained air in the water flow at high velocities is correlated with the air discharge for self-aeration; failure to allow for the air discharge will lead to errors when using empirical equations and to disagreement with the actual test data.

The amount of air entrained by turbulent water flow in a horizontal conduit is thought to depend on the Froude number (USACE 1977; Najafi and Zarrati 2010). Such dependence is likely to be true for inclined penstocks (Figures 1-2 and 2-2a-b). In summary, both the dimensionless Froude number and proper length scales are important for studies of air entrainment and pressure drop in penstocks.

Jaramillo and Villegas (1988) made measurements of air demand from a 1:25 physical model as well as a prototype of a 412-m long penstock. The penstock had cross section area of 21.5 m^2 and a slope of 1.93%. Aeration was provided by a 1.2-m diameter air duct that fed distributor ducts around the gate. A separate conduit parallel to the penstock with five 0.6-m diameter holes provided aeration downstream of the gate. Measurements of air flow from the reduced scale model were made using a hot wire anemometer located in the aeration conduit. The downstream end of the conduit was blocked with an adjustable gate that prevented air from re-entering the conduit. Prototype measurements were obtained using industrial air flow meters. The model measurements were reported to fit well with an existing empirical relationship. It was not possible to validate the model measurements using the prototype measurements because air was observed to re-enter the penstock during the prototype measurements. This renders the results inconclusive.

McKee et al. (1996) investigated the time-dependent water and air flow in a penstock caused by closing the head gate by means of mathematical modelling. They used simple global arguments on the basis of mass conservation and momentum balance. From the time-dependent Bernoulli equation, the investigators derived evolution equations for the fluxes of water and air through the various components of the system. They also solved the time-dependent Navier-Stokes equations. However, their solutions corresponded to a substantially reduced Reynolds number, which is a significant limitation. The investigators suggested that the pressure in the penstock remained above one half of the standard atmospheric pressure (101.325 KPa). A limitation of their study is that the model domain is simple and highly idealised, not necessarily reflecting the geometry of real-world penstocks.

3. ANALYSIS METHODS

3.1 Intake Gate Closure

Stoney gates (Figures 2-2a,b) are the most common head gate used in hydropower plants in Quebec. These gates are raised and lowered through a gate well. The gate well is located in the upstream section of the hydraulic passage between the intake and penstock. A Stoney gate is a type of crest gate that is capable of moving up and down and on which rollers or wheels are attached and roll on a fixed surface (Mark and Gross 2011) in a gate well or gate rack, as opposed to other types of gates that roll on wheels attached to a fixed surface.

For a Stoney gate, the seal can be achieved in two configurations, namely an upstream seal configuration (Figure 2-2a) and a downstream seal configuration (Figure 2-2b), in which the seals are lined up vertically with the upstream face and the downstream face of the gate well, respectively. When the penstock is drained, the gate well of an upstream seal gate configuration (Figure 2-2a) will also be drained, while in a downstream seal configuration (Figure 2-2b) the water level in the gate well will be the same as the water level in the upstream reservoir. Downstream seal hydraulic passages require air vents, while upstream seal configurations generally do not. In normal operating conditions, the water level inside the gate well tends to be lower than the water level in the upstream reservoir due to the head loss across the intake structure.

In case of an emergency closure, the head gate (or the Stoney gates in Figures 2-2a,b) instead of the wicket gates is used to interrupt the flow. The process is almost never automated due to safety purposes. It is our understanding that operators of major stations in Canada are aware of this maneuver and are prepared to use it if needed.

Let w_o denote the gate opening (in m) under normal operation, and T denote the time (in s) it takes to complete an emergency closure. If the closing proceeds at a constant pace, the gate opening w at any given time t is given by

$$[3.1] \quad w = w_\circ\left(1-\frac{t}{T}\right) \qquad \text{for } 0 \le t \le T$$

It is common to find two intake structures for one generating unit in which a Y-shaped penstock (Figure 3-1) is used to convey water to the turbine. In such a case, the operators are to follow a specified sequence of closure with a certain delay between the successive activation of the two gates in order to assure they will not close at the same time. Site visits to Hydro-Quebec power- generating stations indicate that not a single emergency closure procedure was based on scientific studies. The current practice was rather based on a mixture of logics and "gut feeling". This is mainly because there is a lack of existing methods for determining an ideal sequence.

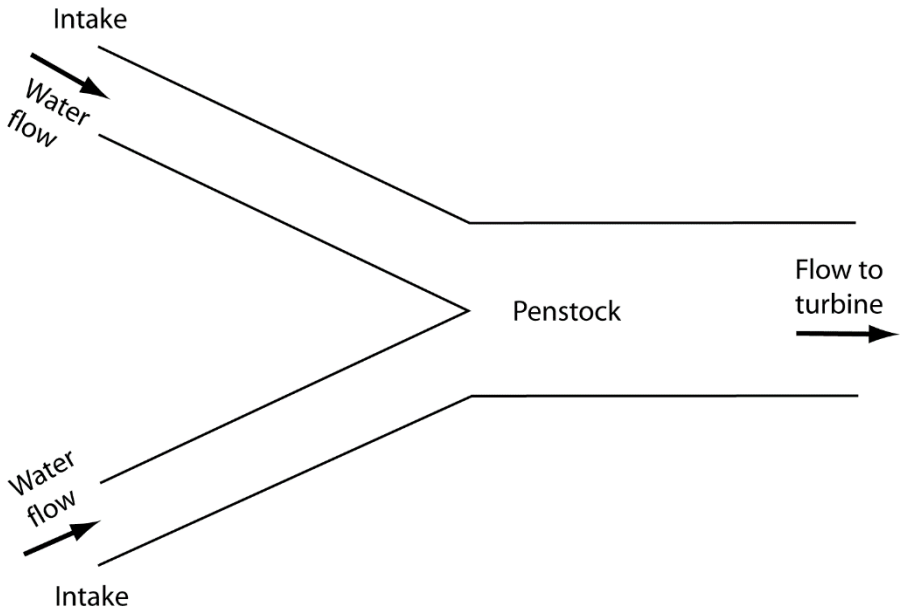

Figure 3-1 A schematic diagram of a Y-shaped penstock (top view).

3.2 The Energy Principle

Consider flow passing underneath a vertical sluice gate (Figure 3-2a-b) in a rectangular channel. The gate is an opening in the base of a large reservoir upstream. Through the opening, water is discharged in the form of a jet. The underflow gate can act like an orifice (Figure 3-2a) or operate under submerged condition (Figure 3-2b). In the case of an emergency closure of the gate, it is important to be able to determine discharge Q (in m^3/s) passing underneath the gate. It is difficult to obtain Q through direct measurements of flow velocity in the region of the orifice or in the jet.

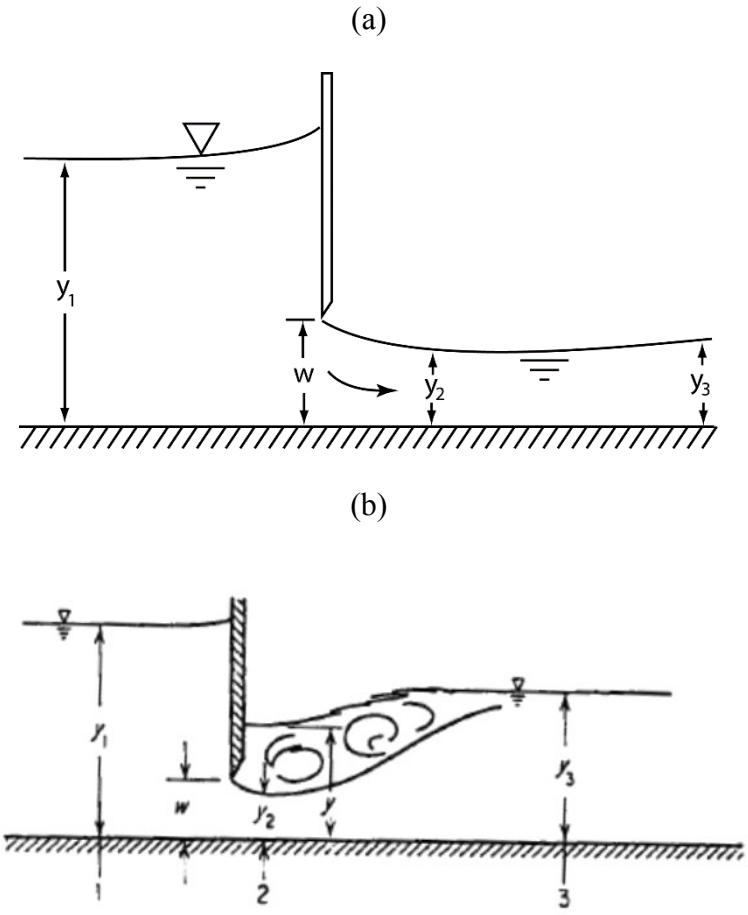

Figure 3-2 A definition diagram of a vertical sluice gate: (a) free flow discharge; (b) submerged flow discharge (adopted from Henderson 1966, p. 208). The sluice gate is in a rectangular channel.

In Figures 3-2a-b, the instantaneous gate opening is w, given in Equation (3-1). The depth of water at cross section 1 well upstream of the gate is y_1. The depth of jet flow at the vena contracta (cross section 2) is y_2. The vena contracta is located at a distance of about 1.15 times w from the gate (Rajaratnam and Subramanya 1967). At this cross section the streamlines of flowing water are parallel. Further downstream at cross section 3 the tail-water depth is y_3. Under submerged condition (Figure 3-2b), the total depth of flow on the downstream side of the gate is y.

The discharge Q will depend on the head of water that produces the flow. That is to say that Q is a function of y_1 (Figures 3-2a-b). Between cross sections 1 and 2 (Figures 3-2a-b), the energy equation may be written as

$$[3.2] \quad z_1 + \frac{v_1^2}{2g} + \frac{p_1}{\gamma} = z_2 + \frac{v_2^2}{2g} + \frac{p_2}{\gamma} + h_L$$

where the subscripts 1 and 2 refer to cross sections 1 and 2, respectively; z is the bed elevation (in m) above a certain reference datum; v is the flow velocity (in m/s); g is the gravitational acceleration (in m/s^2); p is pressure (N/m^2); γ is the specific weight of water (N/m^3); h_L is the energy head loss of water flow between the two cross sections.

In order to determine the functional form of Q, for now, we drop the unknown energy head loss term from Equation [3.2] (or set h_L to zero). We also assume that the channel bottom is horizontal (or $z_1 = z_2$). Accordingly, Equation [3.2] is reduced to

$$[3.3] \quad \frac{v_1^2}{2g} + \frac{p_1}{\gamma} = \frac{v_2^2}{2g} + \frac{p_2}{\gamma}$$

3.2.1 *Discharge of free outflow*

For free outflow, the piezometric head terms are: $p_1/\gamma = y_1$ and $p_2/\gamma = y_2$. Equation [3.3] becomes

[3.4] $$\frac{v_1^2}{2g} + y_1 = \frac{v_2^2}{2g} + y_2$$

By means of continuity for flow in a rectangular channel, the velocities at cross sections 1 and 2 are given by

[3.5a,b] $$v_1 = \frac{q}{y_1} \qquad \text{and} \qquad v_2 = \frac{q}{y_2}$$

where q is the discharge per unit width of channel (in m^2/s). Substituting Equations [3.5a,b] into Equation [3.4] gives

[3.6] $$\frac{q^2}{2gy_1^2} + y_1 = \frac{q^2}{2gy_2^2} + y_2$$

which can be simplified into

[3.7] $$q = y_1 y_2 \sqrt{\frac{2g}{y_1 + y_2}}$$

If the depth of water at cross section 1 is much larger than the depth of flow at cross section 2 (Figure 3-2a-b) or $y_1 >> y_2$, Equation [3.7] can be approximated as

[3.8] $$q = y_2 \sqrt{\frac{2gy_1}{1 + y_2 / y_1}} \approx y_2 \sqrt{2gy_1}$$

For convenience, a reference velocity v_o may be defined as $v_\circ = \sqrt{2gy_1}$. It is important to note that this velocity does not actually occur anywhere in the channel (Henderson 1966). The result given by Equation [3.8] has excluded the effects of energy head loss h_L.

3.2.2 *Discharge of submerged outflow*

For submerged outflow, the piezometric head term at cross section 1 is the same as that for free outflow or $p_1/\gamma = y_1$, but this term at cross section 2 must be equal to the total depth of flow or $p_2/\gamma = y$ (Henderson 1966). Thus, the energy principle (Equation [3.3]) is expressed as

$$[3.9] \quad \frac{v_1^2}{2g} + y_1 = \frac{v_2^2}{2g} + y$$

As in the case of free outflow, the flow velocities at cross sections 1 and 2 (Figure 3-2b) are given by Equations [3.5a,b]. Note that v_2 is the flow velocity through part of the flow section (cross section 2); this part is actually the depth of jet flow. The water mass above the jet depth is considered to be stagnant since the water mass has no net motion in any direction although it is turbulent (Henderson 1966). Therefore, the energy principle (Equation [3.10]) can be rewritten as

$$[3.10] \quad \frac{q^2}{2gy_1^2} + y_1 = \frac{q^2}{2gy_2^2} + y$$

From the above equation, the per unit width discharge is obtained as

$$[3.11] \quad q = y_1 y_2 \sqrt{\frac{2g(y_1 - y)}{y_1^2 - y_2^2}}$$

If $y_1 >> y_2$, as an approximation, the discharge per unit width of channel q is given by

$$[3.12] \quad q = y_2 \sqrt{\frac{2g(y_1 - y)}{1 - y_2^2 / y_1^2}} \approx y_2 \sqrt{2g(y_1 - y)}$$

Similar to free outflow, another reference velocity may be defined as $v_\circ = \sqrt{2g(y_1 - y)}$.

3.2.3 *Maximum depth of tail-water for free outflow*

Between Equations [3.8] and [3.13] or equivalently between Equations [3.9] and [3.14], there is a difference in discharge q determined on the basis of the energy principle (Equation [3.2]), depending on whether the outflow is under free outflow or submerged outflow condition. For free outflow, the allowable maximum value of the tail-water depth y_3 (Figure 3-2a) can be derived from the momentum principle (Henderson 1966, p. 69)

$$[3.13] \quad \frac{(y_3)_{\max}}{y_2} = \frac{1}{2}\left(\sqrt{1+8F_2^{\,2}} - 1\right)$$

where F_2 is the Froude number evaluated at the vena contracta (Figure 3-2a, cross section 2) or

$$[3.14] \quad F_2 = \frac{v_2}{\sqrt{gy_2}} = \frac{q}{\sqrt{gy_2^3}}$$

Munson et al. (2002) gives a physical interpretation of the Froude number as "a measure of, or an index of, the relative importance of inertial forces acting on fluid particles to the weight of the particle. Note that the Froude number is not really equal to this force ratio but is simply some type of average measure of the influence of these two forces".

Equation [3.13] contains three independent quantities: y_2, F_2 and $(y_3)_{\max}$. This equation allows the downstream tail-water depth $(y_3)_{\max}$ to be calculated from the upstream hydraulic condition (y_2 and F_2) at cross section 2 (Figure 3-2a). As Henderson (1966) pointed out, hydraulically speaking, the downstream tail-water depth is caused by some control acting further downstream (for example, the turbine, Figures 2-2 and 3-2), not by the upstream hydraulic conditions.

Traditionally, the depth of jet outflow y_2 under both free and submerged conditions is related to the gate opening w through a general contraction coefficient C_c as

$$[3.15] \quad y_2 = C_c w$$

Thus, Equation [3.13] can be rewritten as

$$[3.16] \quad \frac{(y_3)_{\max}}{w} = \frac{1}{2} C_c \left(\sqrt{1 + 8F_2^{\,2}} - 1 \right)$$

A widely accepted value for the discharge coefficient is $C_d = 0.611$.. Values for the Froude number F_2 depend on the gate opening w relative to the depth of water upstream of the gate y_1 as well as the energy head loss h_L between cross sections 1 and 2. The distinguishing condition given in Equation [3.8] can further be developed with the effects of energy loss taken into account (or $h_L \neq 0$), as discussed in Habibzadeh et al. (2011).

3.3 Underflow Gate Classification

For a given value of the Froude number F_2, Equation [3.16] is valid for determining the allowable maximum tail-water depth $(y_3)_{\max}$ for free outflow. If the actual tail-water level rises such that $y_3 > (y_3)_{\max}$, the jet outflow will be submerged as illustrated in Figure 3-2b. This distinguishing between free and submerged outflow conditions is shown by the virtually straight line in Figure 3-3; it is understood that the result is theoretical.

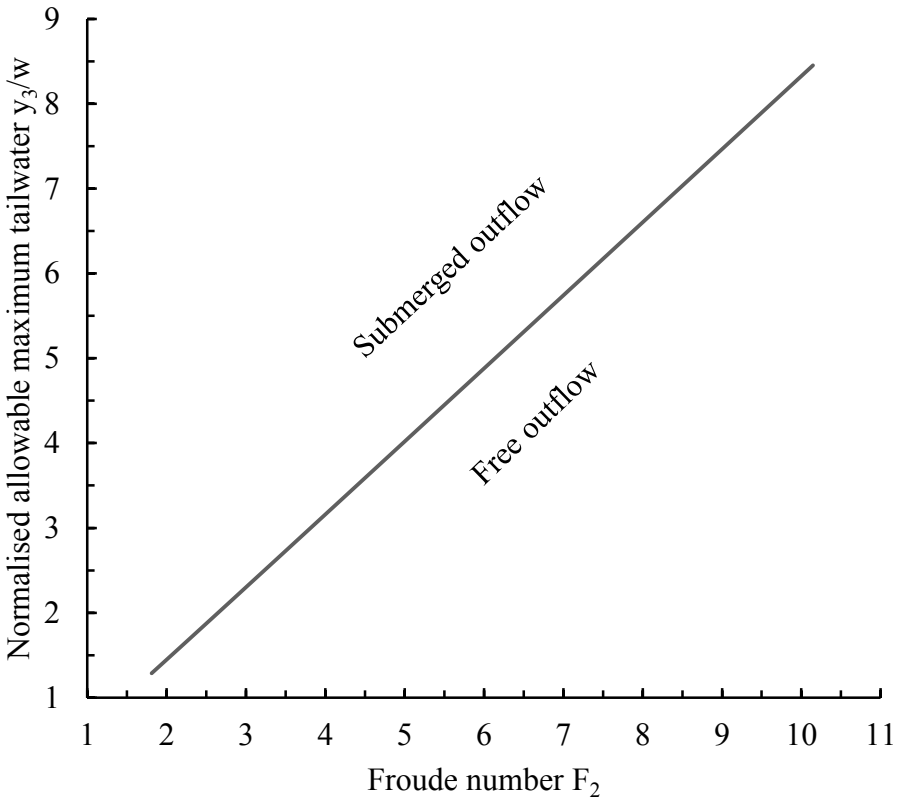

Figure 3-3 Distinguishing condition between free and submerged flows passing a sluice gate.

Since the distinguishing condition (Figure 3-3) involves the depth-to-opening ratio y_1/w through F_2, an alternative way to classify the outflow is to use y_3/w and y_1/w directly. For this reason, a submergence ratio is defined in this study as

[3.17] $$s = \frac{y_3 - w/2}{y_1 - w/2} \qquad \text{or} \qquad s = \frac{y_3/w - 1/2}{y_1/w - 1/2}$$

The denominator and numerator represent the heads on the centreline line of the gate opening on the upstream and downstream sides of the gate, respectively. The ratio s is a dimensionless parameter.

Using this dimensionless parameter, the outflow is classified as follows:

- If $s < 0.67$, the outflow is considered to be under free flow condition.
- If $s > 0.80$, the outflow is considered to be under fully submerged flow condition.
- If $0.67 \leq s \leq 0.80$, the outflow is considered to be under transitional condition.

The specific s values mentioned above for outflow classification were suggested by Bruner (2010, Chapter 8, p. 8-9). The submergence ratio s is more practical to use for outflow classification than $(y_3)_{max}$ given by Equation [3.16].

3.4 Sluice Gate Discharge with Influences of Energy Losses

Between cross sections 1 and 2 (Figures 3-2a-b), energy head losses occur due to friction in the bottom boundary layer, energy transferred from the main flow to turbulent vortices near the surface on the upstream side of the sluice gate and dissipated by small scale turbulent motions, and energy dissipation by turbulent eddies in the contracting jet flow between the gate and the vena contracta.

These energy losses inevitably reduce the energy head available to produce flow beneath the sluice gate. As a result, for a given upstream head y_1 (Figures 3-2a-b), the actual discharge underneath the gate will be lower than the theoretical value of discharge determined from Equation [3.8] under free outflow condition and from Equation [3.12] under submerged outflow condition.

3.4-1 *Free outflow* (*the submergence ratio s* < 0.67)

The tail-water has no impact on discharge Q through the gate opening (Figure 3-2a). Substituting the contraction relationship (Equation [3.15]) into Equation [3.8] gives $q = C_c w\sqrt{2gy_1}$. Let B

denote the width (in m) of the channel. By introducing the discharge coefficient C_d to reflect the effects of energy head losses and streamline contraction at cross section 2, we obtain the following equation for Q

[3.18] $$Q = C_d B w \sqrt{2 g y_1}$$

The discharge given by Equation [3.18] is time-dependent because of the changing gate opening (Equation [3.1]).

3.4-2 *Fully submerged outflow* (*the submergence ratio s* > 0.80)

The level of tail-water on the downstream side of the gate will have a direct impact on discharge Q. Similar to the case of free outflow, the discharge coefficient C_d is introduced to allow for the effects of energy losses and flow contraction on discharge, but under the fully submerged outflow condition, the use of C_d also incorporates the effects of submergence. From Equations [3.15] and [3.12], the discharge is obtained as

[3.19] $$Q = C_d B w \sqrt{2 g (y_1 - y)}$$

The discharge coefficient C_d in Equation [3.19] has values significantly different from that for free outflow. Experimental data reported in Henry (1950, in Henderson 1966, p. 228) show that the discharge coefficient C_d depends on mainly two parameters:

- The ratio of the vertical depth of water on the upstream side of the gate to the height of gate opening, y_1/w
- The ratio of the vertical depth of water on the downstream side of the gate to the height of gate opening, y_3/w.

The experimental data covers parameter values in the range of $2 < y_3/w < 8$ and $2 < y_1/w < 16$. Values for C_d change rapidly with the parameters, from 0.1 to close to 0.6. For example,

$C_d \approx 0.22$ for y_1/w = 8 and y_3/w = 7, the corresponding submergence ratio being s = 0.87 (Equation [3.17]). Values for C_d under submerged flow approach asymptotically C_d values under free flow. No data of C_d is available for the case of y_3 is smaller than twice the gate opening.

3.4-3 *Transitional outflow* (*the submergence ratio* 0.67 < *s* < 0.80)

The underflow gate is considered to be under transitional condition between free outflow and fully submerged outflow. The following equation is proposed for calculating the discharge Q

[3.20] $$Q = C_d Bw(5.5 - 5.63s)\sqrt{2g(y_1 - y_3)}$$

The basic idea of determining Q using the above equation is to produce a smooth discharge curve between free outflow discharge (Equation [3.18]) and fully submerged outflow discharge (Equation [3.19]). Setting the submergence ratio s = 0.80 in Equation [3.20] will recover Equation [3.19], whereas setting s = 0.67 and using the limiting value of $y_3 \approx (2/3)y_1$ for free outflow will recover Equation [3.18].

3.5 Water Level in Air Vents

The water level or equivalently the height of water column, h, in an air vent (Figure 3-3) is an important quantity. In an emergency closure, as the gate begins to drop in a penstock, the blades of the gate quickly enter the upstream part of the penstock. This creates an increasingly larger restriction and therefore causes energy head losses to water flow beneath the gate. In an upstream seal configuration (Figures 2-2a and 3-4), the increase in head loss manifests itself in the form of a lowering water level in the gate well. The drop in water level is equal to the additional head loss. In a downstream seal configuration (Figure 2-2b), the same phenomenon is expected to occur in the air vent. Henceforward, a gate well of upstream seal configuration (Figures 2-2a and

3-4) is referred to as an air vent because it provides the same function with respect to air conveyance to and from the penstock when designed accordingly.

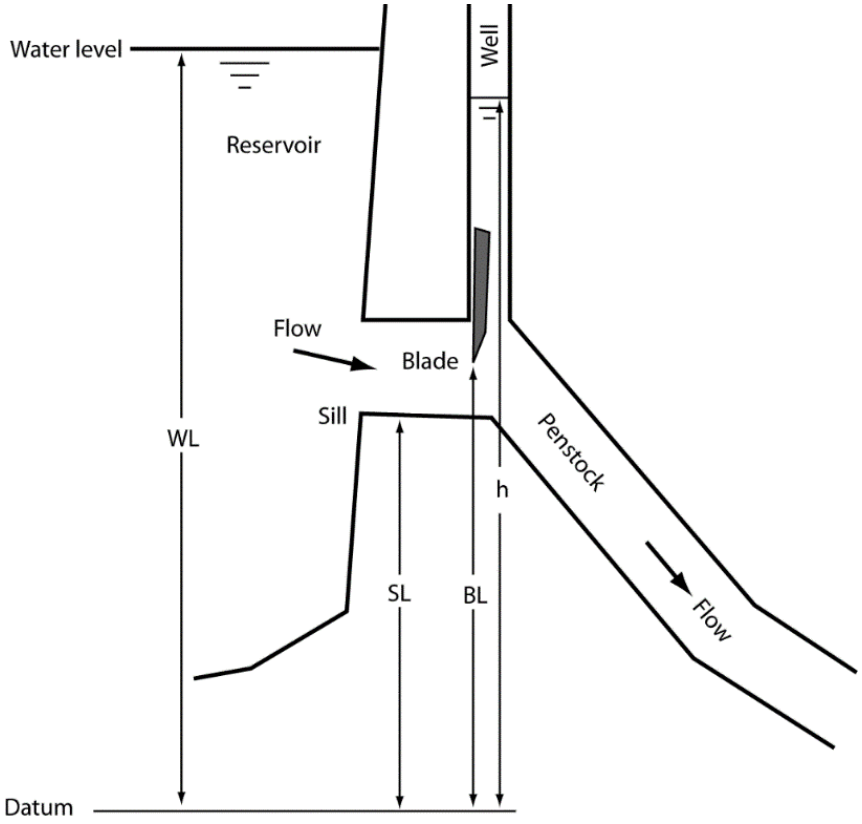

Figure 3-4 A definition diagram of a penstock, with a gate of upstream seal configuration.

As the head gate closes, the water level in the air vent will continue to drop until the air vent is completely dry. The water level downstream of the head gate then reaches the junction between the air vent and the penstock (Figures 2-2a-b).

Let V denote the volume of water in the penstock and air vent. Variations in V with time is governed by the equation of continuity of the form $dV/dt = Q - Q_{out}$, where the discharge Q beneath the gate is calculated using Equation [3.18], [3.19] or [3.20], and Q_{out} is the volumetric rate of flow exiting the penstock through the turbine, which is time-dependent in intake-gate

closure. This continuity equation may be integrated over time to yield updated water volume in the penstock as

[3.21] $V^{n+1} = V^n + (Q - Q_{out})\Delta t$

where the superscripts n and n+1 refer to the current and new time steps, respectively.

The height of water column, h, in the air vent can be related to the volume of water, V, as $h = G(V)$, if the following quantities are given: (1) the diameter, length and slope of the penstock (Figure 3-4), and (2) the diameter of the air vent. The water level-volume relationship may be used to update h at the new time step as

[3.22] $h^{n+1} = G(V^{n+1})$

It is worth noting that the circular model penstock used in this study resembles those at many real-world hydroelectric generating stations. An example of such stations is shown in Figure 3-5.

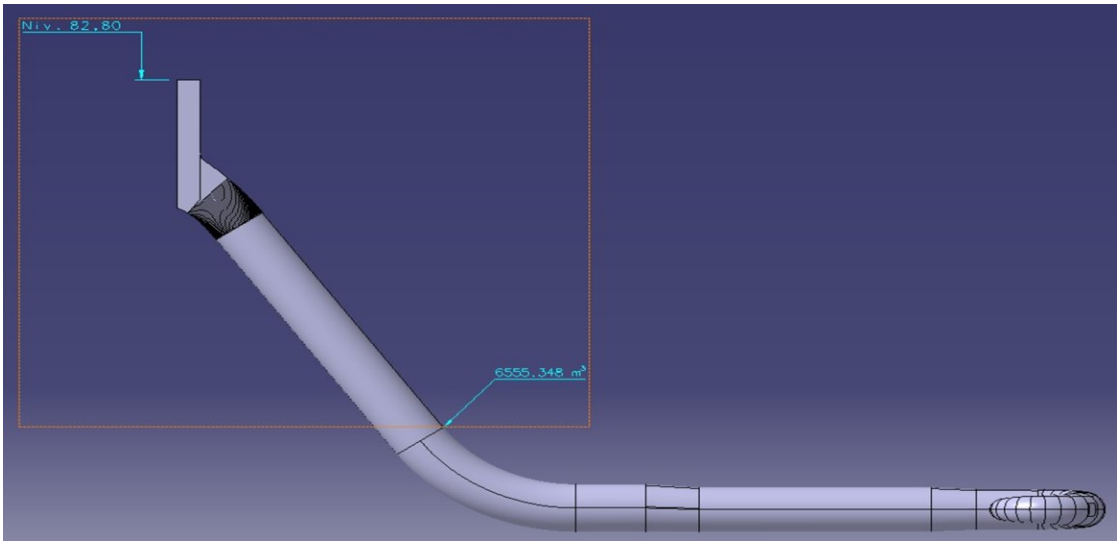

Figure 3-5 A side view of a circular model penstock, with specific characteristics.

Figure 3-6 An aerial view of the Revelstoke Dam in British Columbia. Five penstocks are shown to hug the slope side of the dam (adopted from B.C. Hydro).

3.6 Pressure Head across the Gate

Relative to the centreline of the gate opening or the middle between the gate blades and gate sill (Figure 3-4), the pressure head on the upstream side of the gate is

$$[3.23] \quad \left(\frac{p}{\gamma}\right)_{up} = WL - \frac{BL + SL}{2}$$

where *WL*, *BL* and *SL* are, respectively, the elevations of the upstream water surface, the blades and the water-intake sill (Figure 3-4) relative to an arbitrary datum. The pressure head on the downstream side of the gate is

$$[3.24] \quad \left(\frac{p}{\gamma}\right)_{down} = h - \frac{BL + SL}{2} + \frac{p_a}{\gamma}$$

where $\left(\frac{p}{\gamma}\right)_{down}$ is the air pressure head drop inside the air vent-penstock system. The gross turbine head (or the vertical distance between intake and turbine) is

[3.25a] $(p/\gamma)_t = h - WL_{down} + \frac{p_a - p_{atm}}{\gamma_a}$

where WL_{down} is the water level (tailrace) downstream of the turbine. The discharge through the turbine will be:

[3.25b] $Q_{out} = Q_{11}(p/\gamma)_t^{Z}$

where Q_{11} is the turbine discharge coefficient; the exponent Z is the power coefficient (Values of Z are in the range of 0.3 to 0.55). Both values are determined by curve fitting a selected region of the performance hill chart that is either expected to give the most conservative results or represents a region of higher occurrence.

3.7 Air Flow

Air is sucked into the penstock from outside (the atmosphere) through the air vent. The difference in air pressure between inside and outside the penstock is the total head loss of the air flow through the air vent. There are major and minor losses as discussed next.

3.7.1 *Major head loss*

The major head loss, h_f, (in m) for air flow in the air vent due to friction is calculated using the Darcy-Weisbach formula

[3.26] $h_f = f\frac{L}{D}\frac{v_a^2}{2g}$

where f is the friction factor; L is the length (in m) of the air vent (treated as a pipe); D is the diameter of the air vent (in m); v_a is the air flow velocity (in m/s). The friction factor is obtained from the well-known Moody diagram. This requires input of the Reynolds number, R, and characteristic surface roughness k_s. The Moody diagram is based on the Colebrooke-White equation for turbulent pipe flow

[3.27] $$\frac{1}{\sqrt{f}} = -2\log_{10}\left(\frac{k_s}{14.83R} + \frac{2.52}{R\sqrt{f}}\right)$$

which gives an error of less than 4% (Papaevangelou 2010) throughout the transition to turbulent flow portion of Moody diagram.

Since the main objective of this study is to determine the maximum vacuum pressure, and this pressure will cause air flow of great velocity, there is no need for an accurate calculation of laminar air flow which possibly occurs during a certain period of time as air enters the penstock through the air vent. Therefore, the Colebrook-White equation for turbulent pipe flow (Equation [3.27]) is used throughout the entire computing time from zero to maximum air flow.

3.7.2 *Minor head losses*

Due to contraction and expansion of air flow streamlines in the air vent-penstock system, minor head losses are expected to occur. The sum of these losses is given by

[3.28] $$h_m = k\frac{v_a^2}{2g}$$

where k is the coefficient of all minor head losses. The total head loss will be the sum of the major and minor losses or

[3.29] $$h_f + h_m = \left(f\frac{L}{D} + k\right)\frac{v_a^2}{2g}$$

3.8 Void Air Demand

As the water level in the penstock, h, drops, the volume of air, V, located there above the water level is expanded, and therefore the air pressure, p_a, drops below the atmospheric pressure, p_{atm}. This creates a pressure head difference, Δp, and generates a flow of air (Equation [3.31]) that begins its course outside the plant (or in the powerhouse in some cases), goes through the air vent system, and eventually reaches the penstock. By entering the penstock, the air is working towards decreasing the pressure difference. The flow of air will equalise as the pressure difference between the penstock chamber and the outside corresponds to the total head loss of the airflow with the momentum of air mass assumed as being negligible.

Air vents rarely consist of a simple pipe or well that is open to the outside and connected to the penstock. They most often contain geometric features or obstructions that cause minor losses. Examples of such features or obstructions include air dampers, elbows, expansions, contractions, complex manifolds, ladders, covers, protruding inlets and steel grates to name a few. Air vents often utilize an inspection tunnel to reach the outside. Minor losses of energy head are routinely expressed in terms of velocity head. Inside the penstock chamber, the density of air, ρ_a, is interpolated from charts according to air temperature and pressure.

The left hand side of Equation [3.29] must be equal to the difference in pressure head Δp between inside and outside the penstock in question $\left(\Delta p = p_{atm}/\gamma_\circ - p_a/\gamma_a\right)$, which yields

$$[3.30]\quad \Delta p = \left(f\frac{L}{D} + k\right)\frac{v_a^2}{2g}$$

where γ_o and γ_a are the specific weights of air outside and inside the penstock, respectively. Equation [3.30] may be rearranged to give the air flow velocity as

[3.31] $$v_a = \sqrt{\frac{2g\Delta p}{k + fL/D}}$$

In some cases, the coefficients of minor energy head loss depend on pressure head, which can be itself an unknown variable. An air damper is one of such examples; values for the coefficient for this obstruction vary with the pressure head (Arseneault 2007). In some cases, the coefficients vary with time. An air vent comprising a gate well of an upstream seal gate assembly is an example of such a complex system, for which both major and minor head losses vary with time.

The mass of the air inflow entering the air vent during a time interval Δt is

[3.32] $$m_i = \frac{\pi D^2}{4} v_a \rho_\circ \Delta t$$

3.9 Air Entrainment

In high-velocity water flow, air is being transported along with water in the form of air bubbles. This is known as a self-aeration phenomenon. Air bubbles are pulled into the flowing water through the process of air entrainment. Assume that air entrainment within a penstock is caused by similar turbulent conditions as found in hydraulic jumps. For free surface flow in a partially full conduit without hydraulic jumps, USACE (1977, Hydraulic design chart 050-1) suggested a function for the entrained air volumetric flow, Q_o, depending on the Froude number at the vena contracta.

This study makes two modifications to the functional form of the air-to-water volumetric ratio, β, resulting in

[3.33] $$\beta = \frac{Q_o}{Q_{out}} = 0.03 C_f C_j \left(F - 1\right)^{1.06}$$

The first modification is to allow for the effect of geometry downstream of the hydraulic jump by adding the coefficient C_f. The second modification is to avoid considering a jump when water still occupies the air vent by incorporating the coefficient C_j. This coefficient increases linearly from zero, as the lowering water level reaches the junction of the air vent and the penstock; to one as the water level reaches the level where the maximum Froude number is observed (This requires back calculations). The C_j value remains the same until the water level reaches the gate blades where a different equation is used to determine air entrainment. For example, when the water level downstream of the gate is lower than the gate tip, air entrainment is considered to be due to water jet discharged into air (Chanson 2008).

The Froude number F is evaluated at the vena contracta for free flow with the submergence ratio s less than 0.67.

The mass of entrained air flow during the interval of a time step Δt is [3.34a] $m_o = \rho_a Q_o \Delta t = \rho_a \beta Q_{out} \Delta t$. The change of the total mass of air in the penstock is given by

[3.34b] $\Delta m = \left(m_i - \rho_a \beta Q_{out} \Delta t\right)$

A positive Δm corresponds to a net inflow of air mass to the penstock, whereas a negative Δm corresponds to a net outflow of air mass from it. The volume that this net air mass will occupy is given by

[3.35] $\Delta V_a = \dfrac{\Delta m}{\rho_a}$

3.10 Air Pressure

The relationship between the air pressure, p_a, and air volume, V_a, in the penstock is established at each time step according to Boyle's Law. This law states that p_a times V_a is a constant for a given

air mass, at constant temperature. Between the current and new time steps, the law may be expressed as

[3.36] $$(p_a V_a)^{n+1} = (p_a V_a)^n$$

If the water level drops in the penstock air chamber, the air volume will expand and hence the air pressure will decrease. Equation [3.36] holds prior to taking into account inflow of air from outside to inside the penstock (through the air vent), which will lead to an increase in the amount of air inside.

When the volume occupied by the net air mass (Equation [3.35]) is taken into account, Equation [3.36] should be changed to

[3.37] $$p_a^{n+1} = \frac{p_a^n V_a^n}{V_a^n + \Delta V_a^n}$$

This equation shows that if the volume of air in the penstock expands, pressure will decrease and vice-versa. Combining equation [3.35],and [3.37] we obtain

[3.37] $$p_a^{n+1} = \frac{p_a^n \left(V_a^n + \Delta m / \rho_a^n\right)}{V_a^n + \Delta V_a^n}$$

This equation predicts that a positive net mass of air inflow to the penstock and a reduction in air volume in the penstock ($\Delta m > 0$ or $\Delta Va < 0$) will both result in an increase in air pressure in the penstock; otherwise ($\Delta m < 0$ or equivalently $\Delta Va > 0$), the air pressure will decrease. The accuracy of this approximation (Equation [3.37]) depends on the size of the time step as the density ρ is taken from the previous time step for ease of computation rather than a time average.

4. RESULTS AND DISCUSSION

4-1 Characteristics of the Gates and Penstocks

4-1.1 The Isle Maligne station

A mathematical model was developed in 2011 and calibrated using air- and water-flow data from the La Tuque station. The model was adapted to the Isle Maligne station in order to estimate total air demand. The total air demand included void filling air demand as well as air entrainment through the flow in case of emergency closure. The purpose of the analysis was to determine whether or not the 1918 grey cast iron butterfly gate could endure the negative downstream pressure produced in emergency closure. One of the studied scenarios was an emergency gate closure with synchronised group at 100% wicket gates opening, performed by closing the right gate with the left gate already closed. The corresponding internal pressure was computed to drop by 22.6 kPa.

Air demand in emergency closure was measured in 2013 (Hydro Quebec 2013) at the Isle Malign generating station using a number of piezometers on the inner wall of the gates. Each of the two horizontal-axis butterfly intake gates used for emergency closure had the dimensions of 6.78 m by 4-72 m. A downstream control was provided by a Francis turbine and its wicket gates. As in the case of the La Tuque station in 2006, an emergency gate closure with synchronised group at 100% wicket gates opening was performed by closing the right gate with the left gate already closed. Air pressure inside the penstock chamber was measured to peak at 23.9 kPa 235 seconds after the beginning of the gate closure. A Pitot linked to a Rosemont differential pressure meter was setup to record air velocity inside the air vent. This instrument, however, got flooded and produced no results for use.

4-1.2 The La Tuque station

Air demand in emergency closure was measured in 2006 (Hydro Quebec 2006) at the La Tuque generating station using a high velocity air capture hood. This air capture hood was mounted at the entrance of each of the four air vents of Group 11. The air vents are 12 m long and 45.72 cm (or 18 inches) in diameter. The two intake gates used for emergency closure measured 9.30 m by 4-57 m. A downstream control was provided by a Francis turbine and its wicket gates. An emergency gate closure with a synchronised group was performed by closing the right gate with the left gate already closed.

Velocities of air flow were measured through each hood, peaking at 76 m/s and 73 m/s for the two air vents connecting the left penstock chamber to the outside and peaking at 152 m/s and 157 m/s for the two air vents of the right penstock chamber. Pitot tubes and static pressure gauges were also installed two meters down each air vent. However, they each got flooded due to the oscillation of the water in an earlier maneuver and no useful data were produced from these instruments. Integrating the air flows corresponding to the measured velocity time series gives a total volume of entered air; the total volume was 3891 m^3. The total volume of the penstock is 836 m^3. Such a large difference suggests that air was entrained in the flow out of the unit during an emergency closure.

This means that air entrainment by water flowing at high velocity in the penstock is a very important process. This research takes into account the process of air demand and air pressure drop in emergency closure. The total air demand includes void filling air demand as well as air entrainment through the flow. For air entrainment, a relationship between void fraction vs the Froude number was used. The relationship was calibrated by setting coefficient C_f (Equation [3.33]) to 1.61. The computed air pressure drop inside the chamber was around 36 kPa.

4-1.3 Control parameters

Table 4-1 summaries a list of pertinent parameters and their values used in the calculations of air-pressure drop in the penstocks at the La Tuque and Isle-Maligne hydroelectric power generating stations. These parameters and values reflect the following conditions:

1) Physical conditions of the intake gates, penstock chambers and air vents
2) Operational conditions of the upstream reservoirs and downstream tailraces
3) Characteristics of the turbines

Table 4-1 also lists some constants and coefficients. In most of cases, the constants and coefficients are assigned values widely accepted in the literature. Examples include the coefficient of contraction C_c and the coefficient of minor head losses k. The values assigned to the time period (T) it takes to close the gate virtually are based on field measurements in emergency closure of intake gates at the La Tuque and Isle-Maligne stations. The table gives an overview of parameters involved in the determination of time-dependent water discharge underneath an intake-gate, air flow through an air vent, air demand and air pressure drop.

The intake-gate at the La Tuque station is a steel Stoney gate. The intake-gate at the Isle-Maligne station is a horizontal axis butterfly gate made of grey cast iron.

Table 4-1 A summary of control and geometric parameter.

Parameter or constant	La Tuque	Isle Maligne	Equation
Physical conditions			
Equivalent diameter of the air vent D (m)	0.45	0.84	[3.26]
Length of the air vent L (m)	12	14	[3.26]
Quantity of air vents per group	4	1	
Initial gate opening w_o (m)	9.30	6.78	[3.1]
Penstock free width at gate section B (m)	4-57	4-72	
Number of gate per unit	2	2	
Characteristic surface roughness k_s (mm)	0.45	C = 100*	[3.27]
Constants and coefficients			
Density of air outside the air vent ρ_o (kg/m^3) (at 20^{o}C and 101.325 kPa)	1.2041	1.2041	[3.32]
Specific weight of water γ (N/m^3)	9810	9810	[3.2]
Standard atmospheric pressure p_{atm} (kPa)	101.325	101.325	[3.25a]
Gravitational acceleration g (m/s^2)	9.81	9.81	[3.2]-[3.8]
Air-intake coefficient of minor head losses k	0.5	0.8	[3.28], [3.31]
Coefficient of contraction C_c	0.61	varying	[3.15]-[3.16]
Numerical parameters			
Time period of emergency gate closure T (s)	446	420	[3.1]
Time interval for integration Δt (s)	1	0.066	[3.21], [3.32]
Reservoir operation conditions			
Upstream depth of water y_1 (m)	> 20.12	18.60	[3.4]-[3.12]
Water level of the upstream reservoir (m)	152.05	101.54	
Water level downstream of turbine WL_{down} (m)	117.97	67.94	[3.25a]
Turbine characteristics			
Turbine flow coefficients (the ratio $Q11/Z$)	40 / 0.5	46.7 / 0.329	[3.25b]

*For conversion from the Chezy coefficient C to k_s, refer to (Chow 1959).

4-1.4 Water volume - water level relationship

It is understood that penstocks at different hydroelectric power generating stations are likely to have their own features in terms of shape, length, slope and so on (Figure 3-4). Therefore, when applied to a specific station, the general form of Equation [3.22] needs to cast into a specific water volume – water level relationship (or V vs. h relationship, see Figures 1-2b, 2-2b and 3-4). In fact, for the penstock in question, it is desirable to establish the specific relation between V and h because the relation will facilitate calculations of air flow in the air vent and demand air due to void spaces in the penstock.

For the Isle-Maligne and La Tuque stations (Figure 2-2b), the V vs. h relationships have been derived from their actual geometric features. The two relationships are graphically presented as curves in Figure 4-1 and Figure 4-2, respectively. These graphics exhibit a number of characteristics:

1) Along each of the curves, the point of a sudden increase in slope represents the connecting section between the penstock chamber and the air vent (Figure 3-4).
2) The water volume corresponding to the sudden change in slope represents the design capacity of the penstock.

The design capacities of each penstock at the Isle-Maligne and La Tuque stations are close to 2200 and 1400 m^3, respectively. Although the results discussed above are applicable only to specific stations, the approach can be generalized to develop V vs. h relationships for a wide range of penstocks. The level to volume relationship provides the necessary geometric information that is required to achieve the routing needed for the computation of air-pressure drop in emergency closure.

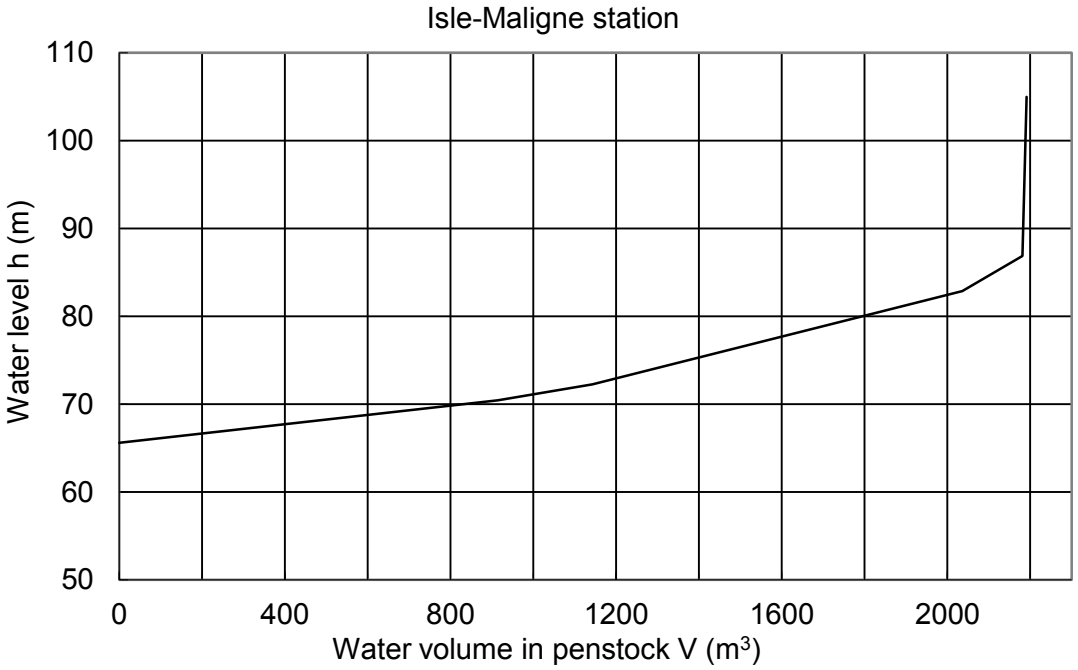

Figure 4-1 Relationship between water volume and water level in the penstock at the Isle-Maligne generating station. The water level is relative to the reference datum (see Figure 3-4).

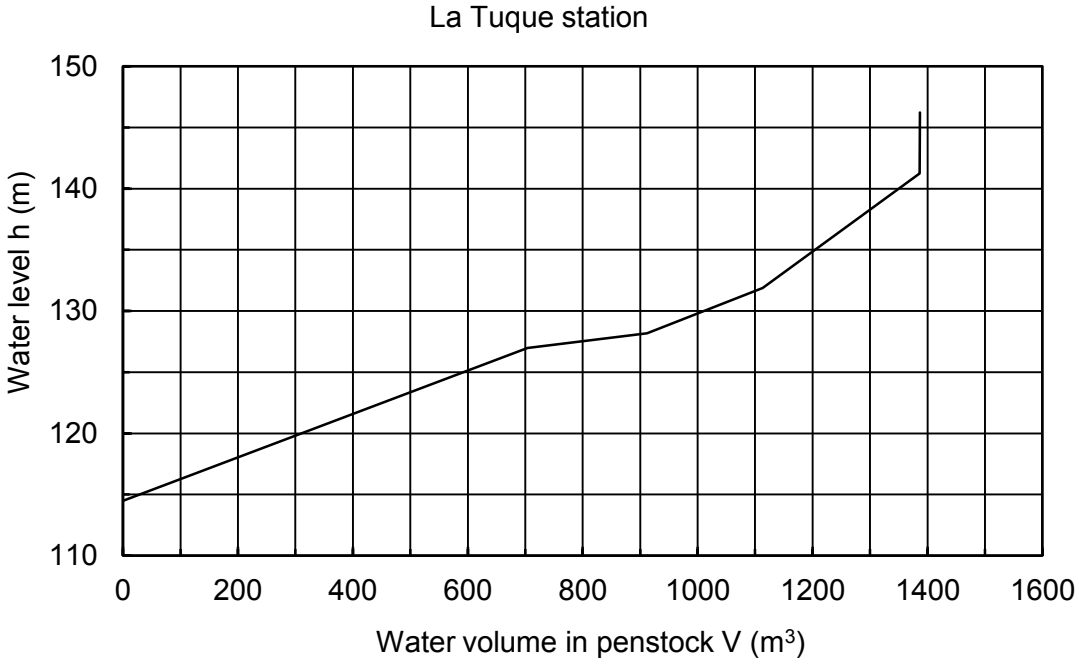

Figure 4-2 Relationship between water volume and water level in the penstock at the La Tuque generating station. The water level is relative to the reference datum (see Figure 3-4).

4-2 Gate Closure Speed

In emergency closure of the intake gate (Figure 1-2), the lowering speed of the gate is approximately constant. This speed can be estimated as the ratio of the initial gate opening, w_o, prior to closing the gate, to the time period it takes to close the gate T (Table 4-1). The estimates are 2.1 cm/s for the sluice gate at the La Tuque station and 2.6 cm/s (equivalent to a sluice gate) for the butterfly gate at the Isle-Maligne station. This speed can perhaps be used as a guideline for an emergency closure of intake gates at other hydroelectric power generating stations.

4-3 Calculated and Measured Discharges

4-3.1 Flow through the Intake Gate at the Isle-Maligne Station

A time series of the calculated intake-gate opening, w, (Figures 1-2 and 2-1b) at the Isle-Maligne station during the progress of an emergency closure of the gate, is shown as the dashed line in Figure 4-3. The calculations use Equation [3.1]. On the vertical axis of the figure, the calculated gate opening has been normalised by the initial value of the gate opening, w_o, prior to closing the gate. This initial value is w_o = 6.78 m. On the horizontal axis of the figure, the time, t, has been normalised by the time period it takes to close the gate. This time period is T = 420 s. The gate opening is seen to reduce from the initial value at the beginning of the closure to zero at the end.

While the intake-gate is being closed, water discharge, Q, underneath the gate (Figures 1-2 and 2-1b) drops. A time series of the calculated Q at the Isle-Maligne station is plotted as the solid curve in Figure 4-3. The calculations use Equations [3.18] – [3.20]. The calculated discharge shown in the figure has been normalised by the initial value of Q prior to closing the gate. This initial value is Q_i = 121.4 m^3/s. This time series shows Q decreasing with time from the initial value to zero.

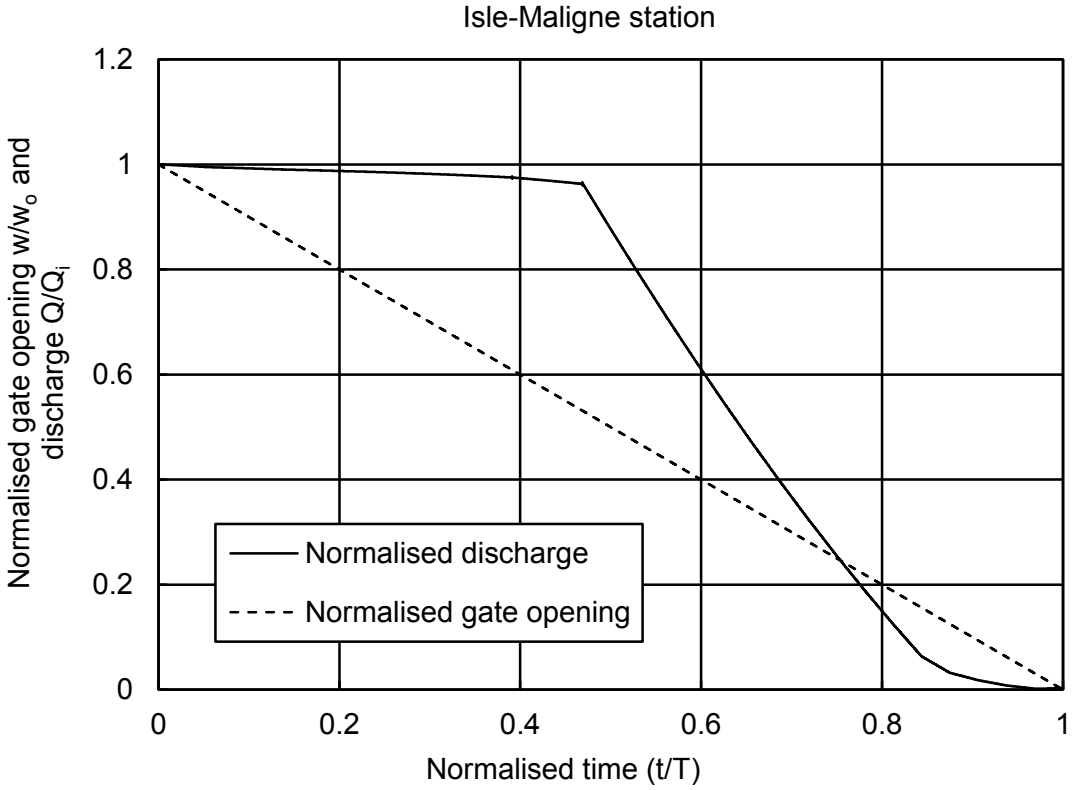

Figure 4-3 Time series of calculated intake-gate opening and water discharge underneath the intake gate of Isle Maligne station. The time period is T = 420 s (Equation [3.1]). Prior to closing gate, the initial gate opening is wo = 6.78 m (Equation [3.1]), and the initial water discharge is Qi = 121.4 m3/s.

Field measurements of the intake-gate opening and water discharge underneath the gate at the Isle-Maligne station are plotted as time series in Figure 4-4. The measurements gave an initial discharge prior to the closure is Q_i = 126.2 m^3/s. Details about the types of instruments used, their precision and field procedures for the measurements have been given in Hydro-Quebec (2013). The calculations (Figure 4-3) are seen to capture the key characteristics of the measurements. There are some minor discrepancies: The measured discharges show smooth transitions, whereas the calculated discharges contain a relatively sharp change at about t/T = 0.47.

It is worth noting that the calculated initial water discharge of Q_i = 121.4 m^3/s is in the close proximity of the measurement (Q_i = 126.2 m^3/s). The accuracy is better than 95%. This indeed indicates that the approximate theory, which is based on the energy principle, can produce relevant and acceptable results. Calculations involved are mainly algebraic, along with time stepping. They are simple and efficient, in comparison to computations of two-phase (air and water) flow based on the momentum principle. Arguably, the analysis method presented in this thesis is adequate for practical estimates of discharge associated with emergency closure of an intake gate in hydroelectric power generating stations. For Isle Maligne station, it is computed that volumetric air entrainment rate is at its maximum when the Froude number reaches 9.27 for the top orifice and 6.76 for the bottom orifice.

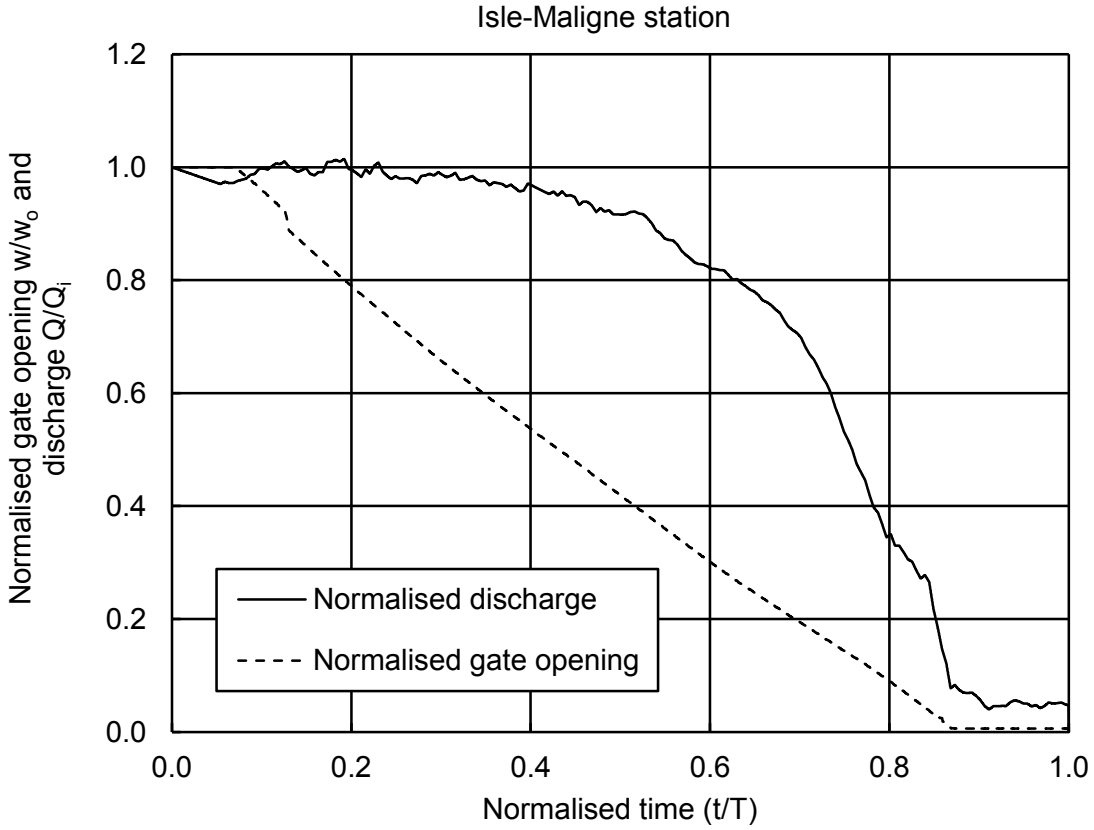

Figure 4-4 Time series of measured intake-gate opening and water discharge underneath the gate at the Isle-Maligne station. The time period is T = 420 s (Equation [3.1]). Prior to closing gate, the initial gate opening was w_o = 6.78 m. The initial water discharge was Q_i = 126.2 m^3/s. The measurements were made in September 2013 (Hydro Quebec 2013).

4-3.2 Flow through the Intake Gate at the La Tuque Station

In Figure 4-3, time series of the calculated intake-gate opening, w, and water discharge, Q, underneath the gate at the La Tuque station are plotted. The calculations use Equations [3.1] and [3.18] – [3.20]. Similar to the data presented in Figures 4-4 for the Isle-Maligne station, the calculated gate opening and water discharge have been normalized (Figure 4-5) by the initial values of the two quantities prior to closing the gate. The initial values are w_o = 9.30 m and Q_i = 220.0 m^3/s. The time period it takes to close the gate is T = 446 s. The two time series show w and Q decreasing from the initial values to zero over the time period. No field measurements of water discharge to gate opening from the La Tuque station are available.

In the first half of the time period when the intake gate is being closed, water discharge drops at a slower rate than the gate opening (Figures 4-3 to 4-5). This means that the cross-sectional averaged velocity of water flow increases with time; in other words, the jet flow intensifies. For example, prior to closing the intake-gate at the Isle-Maligne station, the jet velocity at the gate section (Figures 3-2 and 3-4) is 3.495 m/s, as determined from a discharge of 126.2 m^3/s, a gate width of 4-72 m and a gate opening of 6.78 m (Table 4-1). At half-time of the closure period, the jet velocity at the gate section increases to 8.624 m/s, although the total discharge of water through the gate decreases from the initial value (Figures 4-6 and 4-7). The intensification of water jet will enhance air entrainment in the penstock chamber. For La Tuque station, it is computed that volumetric air entrainment rate is at its maximum when the Froude number reaches 4.71.

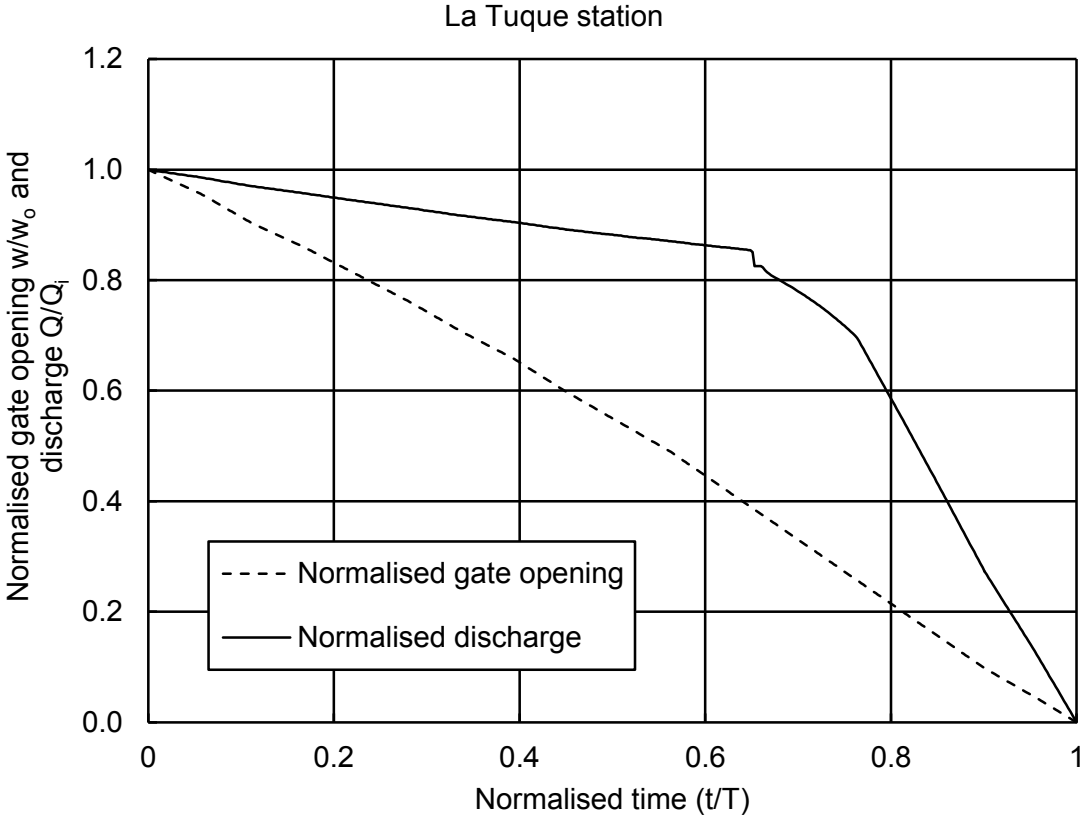

Figure 4-5 Time series of calculated gate opening and discharge underneath the intake gate at the La Tuque station.

4-3.3 Outflow to the tailrace

In Figure 4-6, time series of the calculated intake-gate opening, w, and water discharge, Q, underneath the gate at the Isle Maligne station are plotted, along with outflow through the turbine, Q_{out}. The flow rate of air demand due to void space filling and that due to entrainment by water flow are also plotted. The same quantities are plotted in Figure 4-7 for the La Tuque station.

Calculations of the outflow are based on Equation [3.25b] and hill chart parameters. At both stations, the initial values of Q_{out} are equal to those of the inflow through the intake gates as the gates are fully open. For example, at the La Tuque station (Figure 4-7), the initial Q_{out} is 220.0

m^3/s. The inflow (the thick, dashed curve) overlaps the outflow (the thick, solid curve) until the gate opening reduces to about one-thirds of the initial gate opening (the thin, dashed line). The time period of overlap is about two thirds of the time period (T) it takes to close the gate. This finding is interesting and has implications to proper emergency closure manoeuvres. Over the last one third of the time period T, the thick, solid curve is plotted to the right of the thick, dashed curve, meaning that the outflow exceeds the inflow.

This moment marks the beginning of significant air demand. Air demand due to void space filling and that due to entrainment by water flow remain null until the last third of the time period (Figures 4-6 and 4-7). Air entrainment by flowing water is not allowed in the calculation until the water level descends in the air vent and incoming turbulent flow to the chamber becomes directly in contact with air. This is controlled through the coefficient C_j in Equations [3.33], which is set to one when air reaches the penstock chamber and to zero before that time. This treatment is realistic.

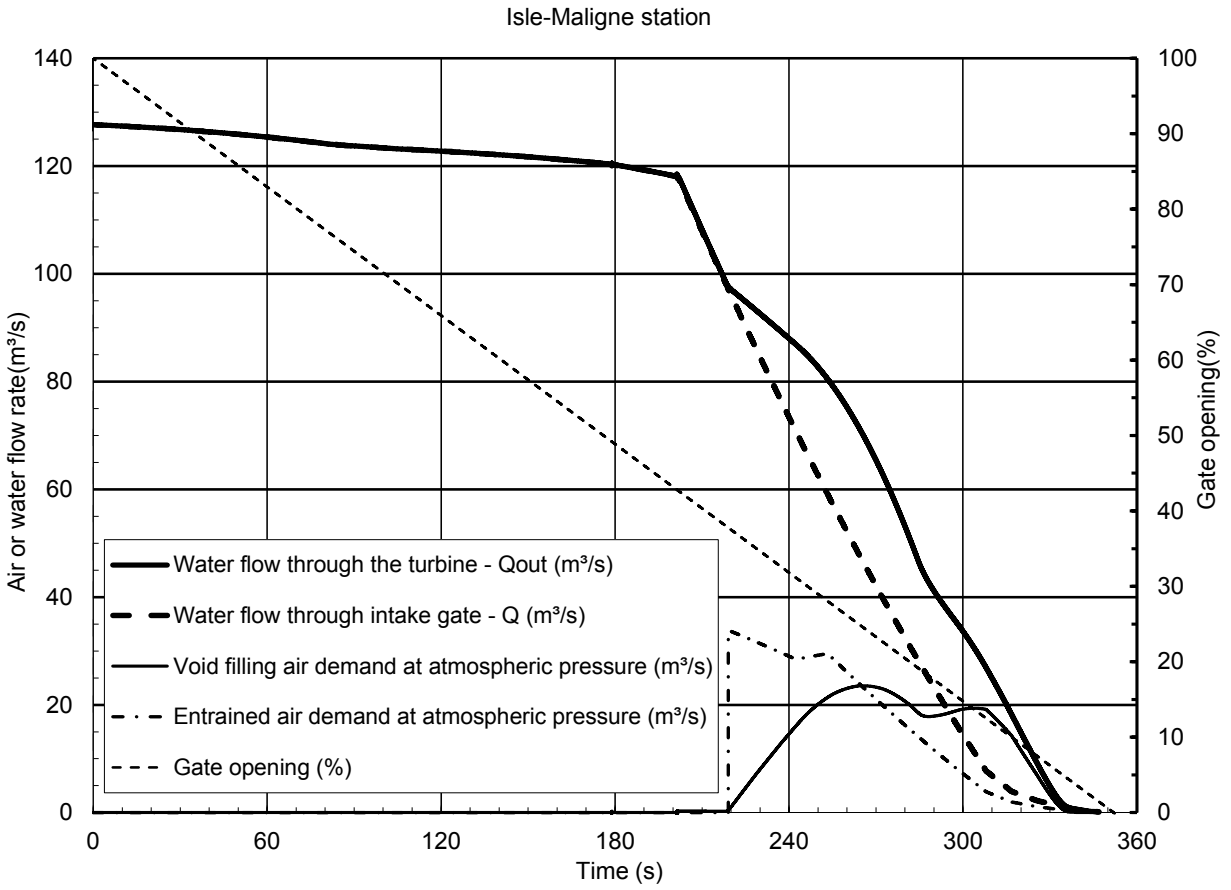

Figure 4-6 Time series of calculated water outflow through the turbine and flow rate of air demand due to void space filling and due to entrainment by water flow at the Isle-Maligne station. The calculated water discharge underneath the intake gate is shown for comparison.

It is interesting to note that the two penstocks have different features but behave in the same manner with regard to inflow and outflow overlap in the first two thirds of the time period of the gate closing (Figures 4-6 and 4-7). The common condition of overlap is greatly dependent on the water level – water volume relationship of the penstock. The particular shapes created between the time series of the inflow and outflow are due to a routing effect. For instance, the separation between inflow and outflow data series occurs when the water level inside the air vent reaches the penstock chamber. One can observe a clear relationship between the vertical distance

between these two curves and the data series of the air demand required to replace the water volume as it decreases.

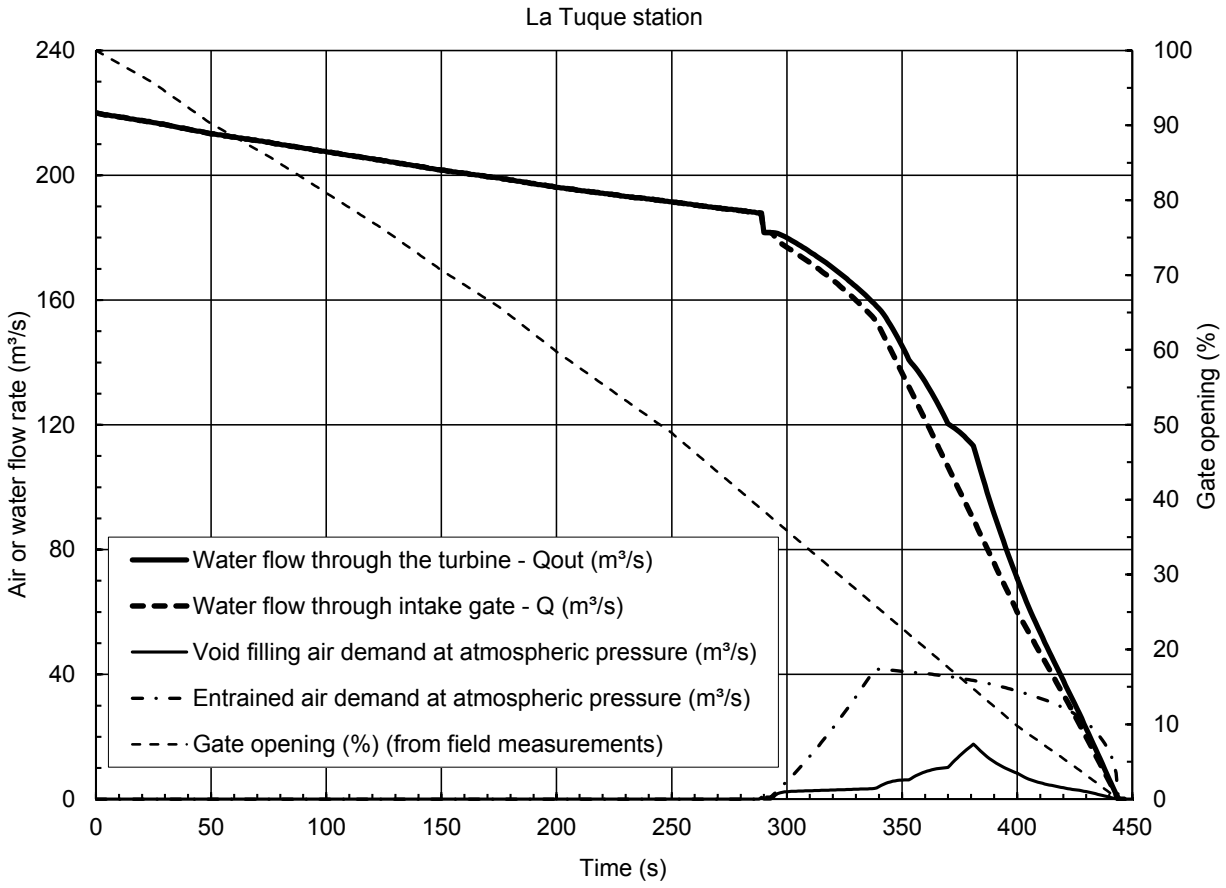

Figure 4-7 Time series of calculated water outflow through the turbine and flow rate of air demand due to void space filling and due to entrainment by water flow at the La Tuque station. The calculated water discharge underneath the intake gate is shown for comparison.

4-4 Relationship of Pressure Drop to Air Flow through Air Vents

As discussion in Section 4-1.4, for a given penstock, the water volume - water level relationship is most likely to be specific, because of the penstock's particular geometric features. Similarly, a given air vent is most likely to have particular geometric features, and specific values for the

coefficients of major and minor head losses (Equations [3.28], [3.31]) are expected. Therefore, it would be necessary and convenient to establish the relationship between pressure drop in the penstock chamber and the volumetric rate of air flow through the air vent. The relationships for the Isle-Maligne and La Tuque stations are graphically shown in Figures 4-8 and 4-9.

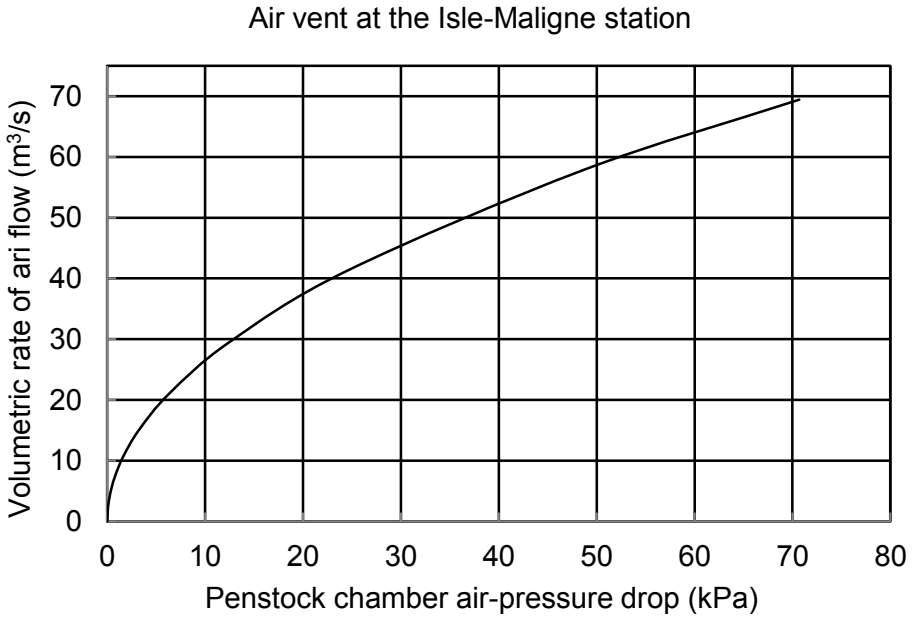

Figure 4-8 Relationship between air-pressure drop in the penstock and volumetric rate of air flow through the air vent at the Isle-Maligne generating station.

On the horizontal axis of Figure 4-8, the air-pressure drop is the atmospheric pressure (p_{atm} = 101.325 kPa) outside the air vent minus the air pressure in the penstock chamber. This difference in pressure will cause air to flow through the air vent at a velocity given in Equation [3.31]. Note that the equation is written in terms of pressure head drop (Δp). On the vertical axis, the volumetric rate of air flow is the air flow velocity times the cross sectional area (Table 4-1) of the air vent.

One way to use the pressure drop - air flow relationship is explained through an example given below: Suppose that the penstock-chamber air pressure, p_a, is below p_{atm} at 70.325 kPa. The pressure difference will be 30 kPa (Figure 4-8). This will cause air inflow to the chamber at a volumetric rate of about 45 m^3/s.

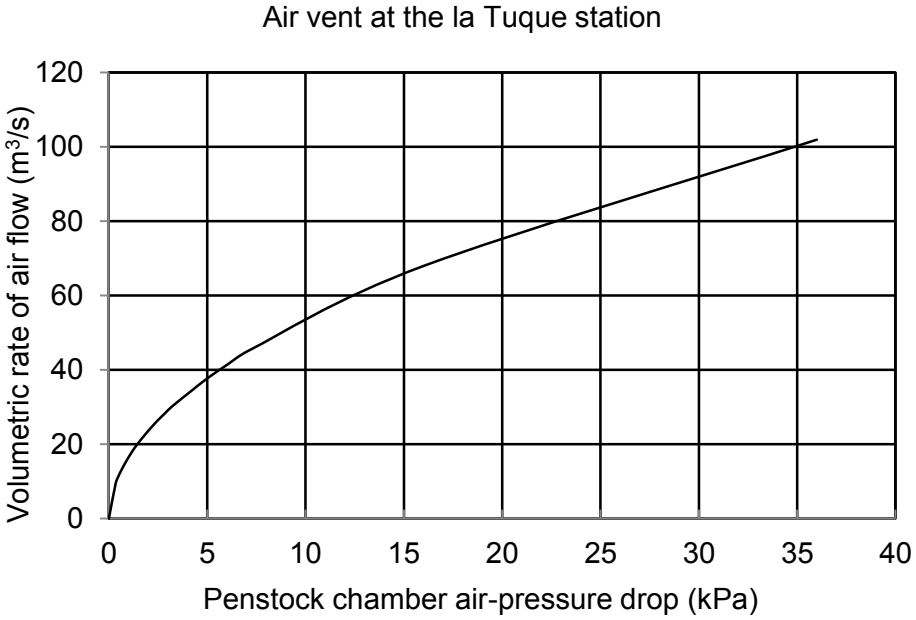

Figure 4-9 Relationship between air-pressure drop in the penstock and volumetric rate of air flow through the air vent at the La Tuque generating station.

Another way to use the pressure drop - air flow relationship is to find the expected pressure drop in the penstock chamber from measurements of air flow through the air vent. At the La Tuque generating station (Figure 4-9), the static pressure gauge installed in the air vent for air pressure measurements got submerged by water. As a result, the air pressure had to be computed from measurements of air-flow velocity and estimated head losses of air flow through the air vent. Note that air velocities were measured using a high-velocity air capture hood. To the best

of my knowledge, this represents the first time to obtain pressure drop that fits such a curve (Figure 4-9) in the manner described above.

4-5 Air Demand and Pressure Drop

In Figure 4-10, a time series of calculated air flow rate (the thick, dashed curve) at the La Tuque station is compared with measurements (the thick, solid curve). Along the two curves, the peak value of calculated flow rates is shown to be in good agreement with the measured peak value. The calculation appears to give a total air volume (the area under the thick, dashed curve) passing through the air vent, too large compared to the measurements (the area under the thick, solid curve). This is mainly because the analysis method developed is intended to capture the peak (or maximum) pressure drop behind the intake gate. The maximum pressure drop is believed to be more critical than the duration of off-peak pressure drops as far as the resultant force on the gate is concerned.

Figure 4-10 also shows a dissection of the computed total air entrainment with void replacement air demand, entrained air without the correction factor (1.61) and the corrected air entrainment demand. These curves reveal the relative importance of the physical processes involved in the problem of pressure drop in penstock chambers.

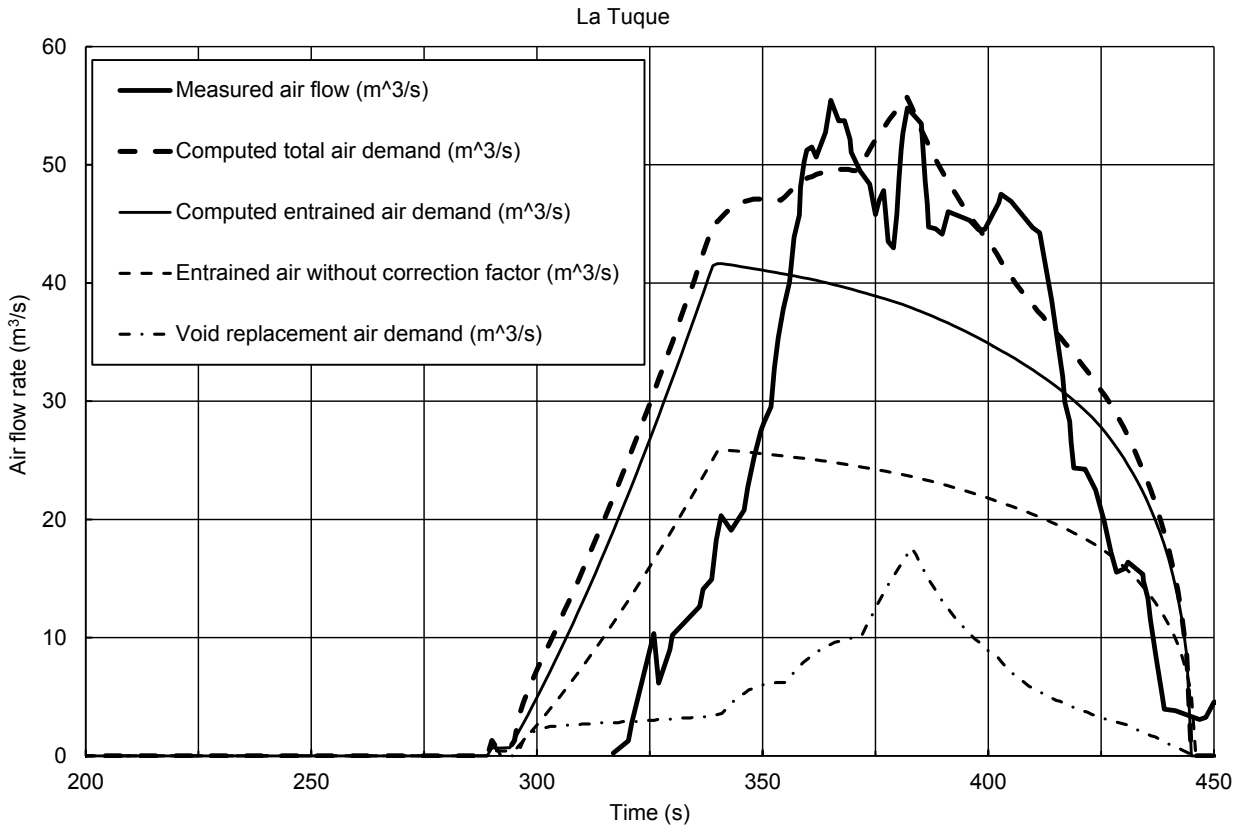

Figure 4-10 Time series of measured and calculated values of air demand at the La Tuque generating station. The calculated values shown correspond to the atmospheric pressure.

Figure 4-11 is the superposition of two time series: One is the measured penstock-chamber internal pressure drop, and the other is the predicted penstock-chamber internal pressure drop. The two series show a good correlation. The measurements show significant fluctuations until the pressure drop reaches the maximum; they also show an offset value of about 1.5% of the atmospheric pressure. There are some discrepancies between the calculated and measured pressure drops. The discrepancies can be improved by adjusting various flow coefficients, head loss curves, and geometry representations in the analysis.

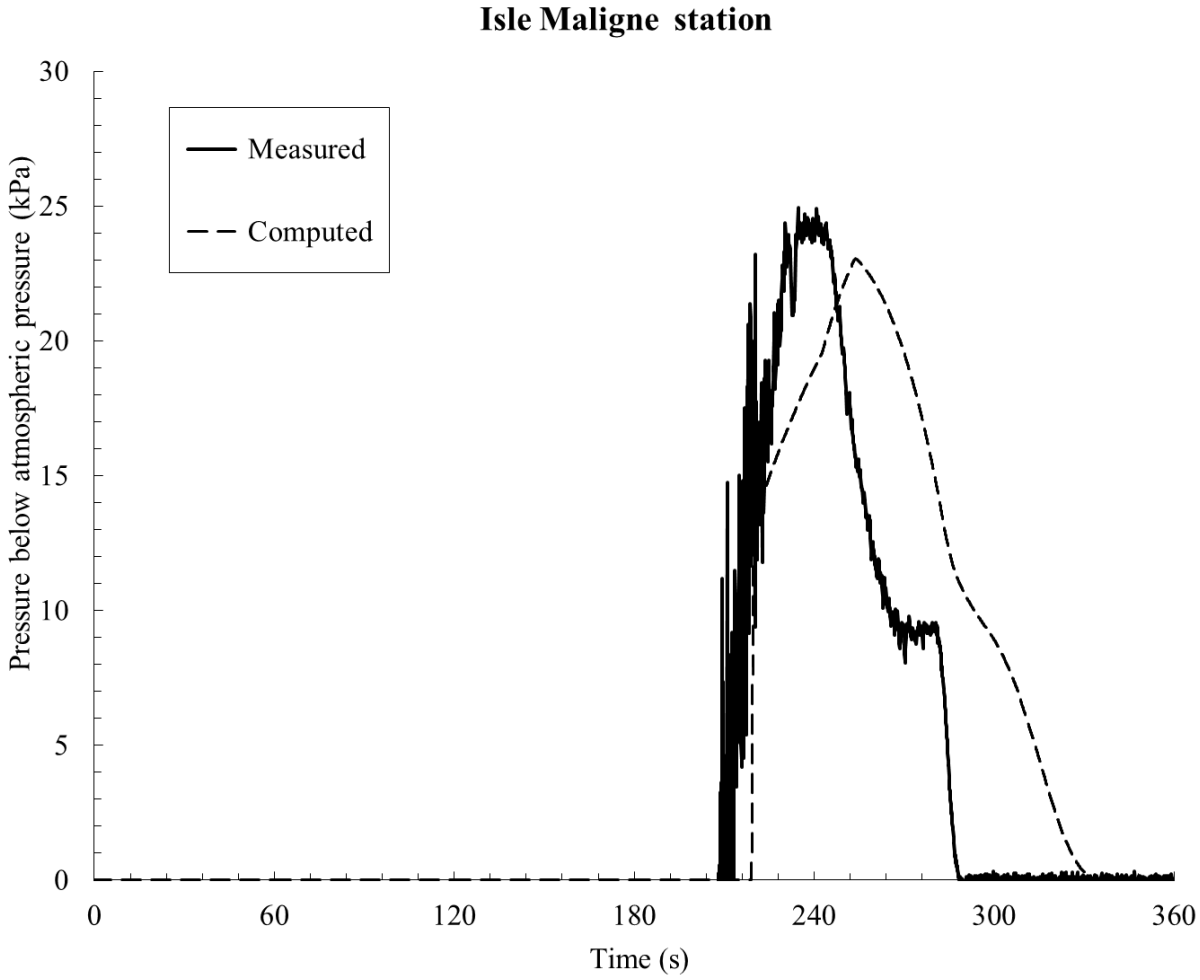

Figure 4-11 Time series of measured and computed air-pressure drop in the penstock chamber at the Isle-Maligne generating station.

It is understood that the pressure field in a penstock chamber contains inherent fluctuations (Figure 4-11) due to the turbulent and chaotic nature of air and water flows there. On the one hand, such fluctuations and pressure offset values seen in the figure point to the difficulties in making field measurements of air pressure and other related parameters from a penstock. Moreover, it is very expensive to make field measurements. On the other hand, the analysis method presented in this thesis is deterministic and therefore is not expected to be able to capture

any fluctuations in the pressure field. However, the overall results from the analysis are acceptable on the time scale of emergency closure of intake gates. The analysis method can be applied to other hydroelectric power generating stations for an appropriate planning and safe operations of emergency closure.

5. CONCLUDING REMARKS

5.1 Summary

This research on the problem of air-pressure drop in a penstock arises from the industrial situation of emergency closure of the intake gates at a hydroelectric power generating station. The quality of existing knowledge about time-dependent air and water flows in emergency closure and about the resultant temporal variations in the pressure field is poor. This research has been conducted to make contributions to filling the knowledge gap.

The research work commences from a review of the pertinent literature. The author proceeds to the development of proper analysis methods, which are based on fundamental fluid mechanics principles. Subsequently, research activities include application of the analysis methods to two hydroelectric power generating stations. The results of air demand and pressure drop from these analyses are compared to valuable field measurements. The author wishes to point out that processing and interpreting the field measurements (raw data) are part of efforts made by author in this research, although the details are not included in this thesis.

Some of the diagrams produced in this study are station-specific, but the ideas about how to produce and use the diagrams are of general significance. They can directly be extended to other stations.

5.2 Conclusions

Prior research on the problem of air pressure drop triggered by closing the intake gates in penstocks is very limited. Field measurements of hydraulic parameters associated with gate closures are extremely sparse. From this research, the following conclusions can be drawn:

1) The analysis methods presented in this thesis are shown to give reliable estimates of air demand and pressure drop in the penstocks at the Isle Maligne and La Tuque stations, triggered by closing the intake gates. There is an excellent agreement between the computed air pressure and measured values, the computed peak value being within 95% of the measurement. Such agreement demonstrates the robustness of the calculation procedures. The accuracy can further be improved by accounting for the peculiarity of the penstock's geometric features.
2) Air entrainment by high-velocity flowing water is an important cause of pressure drop in emergency closure and therefore must be taken into account in order to accurately simulate the process, which has been ignored in some prior studies of the problem of air-pressure drop in a penstock.
3) Air entrainment in the outflow can be modelled using hydraulic jump entrainment equations. This study demonstrates that a coefficient of 1.61 is well suited for the estimation of entrained air demand in an inclined penstock as long as its geometric and operating parameters in the range of the ones of the La Tuque and Isle Maligne hydroelectric power generating stations. Future applications of the analysis methods to other stations should pay close attention to values assigned to this coefficient.
4) In emergency closure of an intake gate, the amount of water discharge underneath the gate does not proportionally reduce to the percentage of instantaneous gate opening. The velocities of the water jet intensify in at the first half of the time period it takes to close the gate, which would produce significant impacts on the penstock structures.

5) Air demand appears to commence when the outflow through the turbine to the tailrace in question exceeds the inflow underneath the intake gate. This occurs mainly in the last one third of the time period of emergency closure.

6) The values of pressure drop calculated for the Isle-Maligne and La Tuque stations are below one third of the standard atmospheric pressure. It is cautioned that the calculation has made no attempt to account for air pressure fluctuations inherently occurring in turbulent and chaotic air and water flows in the penstocks in emergency closure. Given that the fluctuations can be very significant, one should use field measurements and results from mathematical analysis in a complementary manner.

5.3 Suggestions for Future Work

Suggestions for future research on the topic are as follows. Firstly, the present study has introduced a number of assumptions; some of them ought to be dropped for improved estimation of air pressure drop. Second, it would be useful to generalize the calculations involved so that the procedures can directly applied to other hydroelectric generating stations. Third, it would be interesting to carry out computer modeling of the pressure drop problem to cover a wider range of flow and hydraulic conditions as means to extrapolate expensive field measurements.

REFERENCES

Arseneault A. 2007. Volet gravitaire bidirectionnel HARV-607, Essai en soufflerie. Centre de haute technologie Saguenay – Lac St-Jean, Jonquière, P.Q.

Aydin, I. 2002. Air demand behind high head gates during emergency closure. Journal of Hydraulic Research, **40**(1): 83-93.

Borodina, L. K. 1969. Aeration behind low-level gates. Hydrotechnical Construction, **3**(9): 826-834.

Brunner, G. W. 2010. HEC-RAS, River Analysis System Hydraulic Reference Manual. US Army Corps of Engineers, Hydrologic Engineering Center (HEC), Davis, CA. p. 411.

Cassan, L., and Belaud, G. 2011. Experimental and numerical investigation of flow under sluice gates. Journal of Hydraulic Engineering, **138**(4): 367-373.

Colebrook, C. F. 1939. Turbulent flow in pipes, with particular reference to the transition region between the smooth and rough pipe laws. Journal of the Institution of Civil Engineers, **11**(4): 133-156.

Chanson, H. 1991. Aeration of a free jet above a spillway. Journal of Hydraulic Research, **29**(5): 655-667.

Chanson, H. 1996. Air bubble entrainment in free-surface turbulent shear flows. Academic Press. San Deigo, CA. p.348

Chanson, H. 2007. Air Bubble Entrainment in Hydraulic Jumps: Physical Modelling and Scale Effects. In Proceedings of the. 32nd IAHR Biennial Congress, Venice, Italy, G. DI SILVIO and S. LANZONI Editors, Abstacts, Topic C1.b, 10 pages (CD-ROM).

Chanson, H. 2008. Advective diffusion of air Bubbles in Turbulent Water Flows. In Fluid Mechanics of Environmental Interfaces. Taylor & Francis, Leiden, the Netherlands (C. Gualtieri and D. T. Mihailovic eds.), Chapter 7, pp. 163-196.

Chanson, H. 2009. Turbulent air–water flows in hydraulic structures: dynamic similarity and scale effects. Environmental Fluid Mechanics, **9**(2): 125-142.

Chanson, H., and Gualtieri, C. 2008. Similitude and scale effects of air entrainment in hydraulic jumps. Journal of Hydraulic Research, **46**(1): 35-44.

Chawick, A. and Morfett, J. 1993. Hydraulics in Civil and Environmental Engineering, 2nd edition. E & FN Spon, London.

Chin, D. A. 2006. Water-Resources Engineering. 2nd Edition, Prentice Hall, Upper Saddle River, N.J.

Chow, V. T. 1959. Open-Channel Hydraulics. McGraw Hill, Caldwell, N.J.

Clemmens, A. J., Strelkoff, T. S., and Replogle, J. A. 2003. Calibration of submerged radial gates. Journal of Hydraulic Engineering, **129**(9): 680-687.

Côté, E. 2013. Centrale Isle Maligine Group No. 3: Essais de Rupture debit par la vanne Papillion, Hydro-Québec, Montréal, P.Q.

Crane Co. 1982. Flow of fluids through valves, fittings, and pipe. Technical paper No. 410M.Crane Company, New York, N.Y.

Crawford, N. M., Cunningham, G., and Spence, S. W. T. 2007. An experimental investigation into the pressure drop for turbulent flow in 90 elbow bends. Proceedings of the Institution of Mechanical Engineers, Part E: Journal of Process Mechanical Engineering, **221**(2): 77-88.

Douglas, J. F., Gasiorek, J. M., Swaffield, J. A. and Jack L. B. 2005. Fluid Mechanics, 5th edition. Pearson / Prentice Hall, Harlow, UK.

Falvey, H. T. 1968. Air Vent Computations, Morrow Point Dam, Colorado River Storage Project. US Department of the Interior, Bureau of Reclamation, Office of Chief Engineer.

Falvey, H. T. 1980. Air-water flow in hydraulic structures. NASA STI/Recon Technical Report N, 81, 26429.

Gross, M.J., Shiers, P.F., Plisga, A.W., Kropelnicki, J, and Lyon, J.C. 2011. Falls Dam Stoney gate repairs. The 31st Annual USSD Conference, San Diego, CA. U.S. Society on Dams. pp. 691-704.

Gualtieri, C., and Chanson, H. 2007. Experimental analysis of Froude number effect on air entrainment in the hydraulic jump. Environmental Fluid Mechanics, **7**(3): 217-238.

Habibzadeh, A., Vatankhah, A. R., and Rajaratnam, N. 2011. Role of energy loss on discharge characteristics of sluice gates. Journal of Hydraulic Engineering, **137**(9): 1079-1084.

Henderson, F. M. 1966. Open Channel Flow. Prentice Hall, Upper Saddle River, N.J.

Henry, H.R., 1950, Discussion on 'Diffusion of submerged jets', by M.L. Albertson, Y.B. Dai, R.A. Jensen, and H. Rouse:Transactions American Society of Civil Engineers, v. 115, pp. 687-694.

Jaramillo, C. A. and Villegas, A. M. 1988. Air demand of high head sluice gates. In Model-Prototype Correction of Hydraulic Structures, Proceedings of the International Symposium, Colorado Springs, Colorado, August 9–11, 1988 (P. H. Burgi, ed.), pp. 95-101.

Kalinske, A. A., and Robertson, J. M. 1943. Entrainment of air in flowing water: A symposium: Closed conduit flow. Transactions of the American Society of Civil Engineers, **108**(1): 1435-1447.

Lin, C. H., Yen, J. F., and Tsai, C. T. 2002. Influence of sluice gate contraction coefficient on distinguishing condition. Journal of Irrigation and Drainage Engineering, **128**(4): 249-252.

Lorenceau, É., Quéré, D., and Eggers, J. 2004. Air entrainment by a viscous jet plunging into a bath. Physical review letters, **93**(25): 254-501.

Lozano, D., Mateos, L., Merkley, G. P., and Clemmens, A. J. 2009. Field calibration of submerged sluice gates in irrigation canals. Journal of Irrigation and Drainage Engineering, **135**(6): 763-772.

McKee, S., Sneyd, A. D., and Tomé, M. F. 1996. Time-dependent flow in a penstock during head-gate closure. Applied Mathematical Modelling, **20**(8): 614-623.

Munson, B.R., Young, D.F., and Okiishi T.H. 2002. Fundamentals of Fluid Mechanics. John Wiley & Sons, Inc., Hoboken, N.J.

Moody, L. F. 1944. Friction factors for pipe flow. Transactions of the ASME, **66**(8): 671-684.

Najafi, M. R., and Zarrati, A. R. 2010. Numerical simulation of air–water flow in gated tunnels. Proceedings of the ICE-Water Management, **163**(6): 289-295.

Naudascher, E., Rao, P. V., Richter, A., Vargas, P., and Wonik, G. 1986. Prediction and control of downpull on tunnel gates. Journal of Hydraulic Engineering, **112**(5): 392-416.

Nalcor Energy: https://muskratfalls.nalcorenergy.com/construction-activities/muskrat-falls-hydroelectric-generating-facility [accessed 3 March 2013].

Papaevangelou, G., Evangelides, C., and Tzimopoulos. C. 2010. A new explicit relation for friction coefficient f in the Darcy - Weisbach equation. PRE10: Protection and Restoration of the Environment, Corfu, 05-09 July 2010.

Rajaratnam, N., and Subramanya, K. 1967. Flow immediately below submerged sluice gate. Journal of the Hydraulics Division, **93**(4): 57-77.

Sagar, B. T. A. 1995. ASCE hydrogates task committee design guidelines for high-head gates. Journal of Hydraulic Engineering, **121**(12): 845-852.

Sehgal, C. K. 1996. Design guidelines for spillway gates. Journal of Hydraulic Engineering, **122**(3): 155-165.

Sene, K. J. 1988. Air entrainment by plunging jets. Chemical Engineering Science, **43**(10): 2615-2623.

Sharma, H. R. 1976. Air-entrainment in high head gated conduits. Journal of the Hydraulics Division, **102**(11): 1629-1646.

Smit, A. 2007. Air entrainment with plunging jets. M.Sc. thesis, Delft Hydraulics, the Netherlands.

Speerli, J., and Hager, W. H. 2000. Air-water flow in bottom outlets. Canadian Journal of Civil Engineering, **27**(3): 454-462.

Swamee, P. K. 1992. Sluice-gate discharge equations. Journal of Irrigation and Drainage Engineering, **118**(1): 56-60.

Tian, L., Loomis, N., Domínguez-Caballero, J. A., and Barbastathis, G. 2010. Quantitative measurement of size and three-dimensional position of fast-moving bubbles in air-water mixture flows using digital holography. Applied Optics, **49**(9): 1549-1554.

USACE 1977. Hydraulic Design Criteria: Volume 1. United States Army Corps of Engineers, Washington D.C., USA.

Wahl, T. L., 2004. Issues and problems with calibration of canal gates. *In* Critical Transitions in Water and Environmental Resources Management, Salt Lake City, Utah, June 27-July 1 2004. American Society of Civil Engineers, New York, pp. 1-9.

Appendix A - Measurement methodology

for the Isle Maligne Station

Measurement methodology for the Isle Maligne Station

1. Zero setting of instruments

A first reset of all sensors was conducted before the start of the closure, while the valves were positioned horizontally at 12:50 on September 16.

Calibration of the gate position sensors has been achieved during in-air maneuvers, while they were positioned at positions 0 and 100%.

In air pressure sensors reset has subsequently been performed on the morning of September 17 at 10:20, while the ambient atmospheric pressure was about 102.80 kPa according to surrounding weather stations.

2. In-air maneuver

Maneuvers in the air were conducted in the afternoon of September 16. Initially, both butterfly gates were positioned horizontally. For each gate, a closure from that position and an opening from 0 to 100% were recorded. The ranges were shifted to obtain -7 mm when the gate is touching the sill

3. Still water maneuver

Still water maneuver occurred at the end of the afternoon of September 17, first with gate B (left) and then with gate A (right). The test was to open the gate 4 inches and close it.

It was found that the maneuvers were not all made in still water because the penstock was emptied when the valves were closed.

4. Flow interruption

Flow interruption was first made using gate A on September 19. The flow rate to be measured begins from the 20th second of acquisition. The data from 0 to 20 seconds are extrapolated. There is still always a period in which the flow rate is measured before the start of the closing of the gate.

The wire of the submersible pressure gauge in the air vent was cut during the maneuvers.

The pitot tube was turn during the maneuvers and was not lined up with the flow. Water was also found in the tube.

Appendix B - An instrumentation list

for Isle Maligne station measurements

Table A1 - Instrumentation list, instruments 1 to 16.

N° du signal	Nom du signal	Abréviation	Unité	Type de capteur	Plage	Precision
1	Déformation de la vanne B position J1	J1	με	Jauge de déformations submersible uniaxiale en ½ pont HBW-35-250-	≈±1000 με	N/A
2	Déformation de la vanne B position J2	J2	με	Jauge de déformations submersible uniaxiale en ½ pont HBW-35-250-	≈±1000 με	N/A
3	Déformation de la vanne B position J3	J3	με	Jauge de déformations submersible uniaxiale en ½ pont HBW-35-250-	≈±1000 με	N/A
4	Déformation de la vanne B position J4	J4	με	Jauge de déformations submersible uniaxiale en ½ pont HBW-35-250-	≈±1000 με	N/A
5	Déformation de la vanne B position J5	J5	με	Jauge de déformations submersible uniaxiale en ½ pont HBW-35-250-	≈±1000 με	N/A
6	Déformation de la vanne B position J6	J6	με	Jauge de déformations submersible uniaxiale en ½ pont HBW-35-250-	≈±1000 με	N/A
7	Déformation de la vanne B position J7	J7	με	Jauge de déformations submersible uniaxiale en ½ pont HBW-35-250-	≈±1000 με	N/A
8	Déformation de la vanne B position J8	J8	με	Jauge de déformations submersible uniaxiale en ½ pont HBW-35-250-	≈±1000 με	N/A
9	Déformation de la vanne B position J9	J9	με	Jauge de déformations submersible uniaxiale en ½ pont HBW-35-250-	≈±1000 με	N/A
10	Déformation de la vanne B position	J10	με	Jauge de déformations submersible uniaxiale en ½ pont HBW-35-250-	≈±1000 με	N/A
11	Déformation de la vanne B position	J11	με	Jauge de déformations submersible uniaxiale en ½ pont HBW-35-250-	≈±1000 με	N/A
12	Déformation de la vanne B position	J12	με	Jauge de déformations submersible uniaxiale en ½ pont HBW-35-250-	≈±1000 με	N/A
13	Déformation de la vanne B position J13	J13	με	Jauge de déformations rosette submersible branche A en ½ de pont HBWR-35-250-6-SS-HB	≈±1000 με	N/A
14	Déformation de la vanne B position J14	J14	με	Jauge de déformations rosette submersible branche B en ½ de pont HBWR-35-250-6-SS-HB	≈±1000 με	N/A
15	Déformation de la vanne B position J15	J15	με	Jauge de déformations rosette submersible branche C en ½ de pont HBWR-35-250-6-SS-HB	≈±1000 με	N/A
16	Déformation de la vanne A position	J16	με	Jauge de déformations submersible uniaxiale en ½ pont HBW-35-250-	≈±1000 με	N/A

Table A2 - Instrumentation list, instruments 17 to 32.

N° du signal	Nom du signal	Abréviation	Unité	Type de capteur	Plage	Pente
17	Déformation de la vanne A position	J17	με	Jauge de déformations submersible uniaxiale en ½ pont HBW-35-250-6-	≈±1000 με	N/A
18	Déformation de la vanne A position	J18	με	Jauge de déformations submersible uniaxiale en ½ pont HBW-35-250-6-	≈±1000 με	N/A
19	Déformation de la vanne A position	J19	με	Jauge de déformations submersible uniaxiale en ½ pont HBW-35-250-6-	≈±1000 με	N/A
20	Déformation de la vanne A position	J20	με	Jauge de déformations submersible uniaxiale en ½ pont HBW-35-250-6-	≈±1000 με	N/A
21	Déformation de la vanne A position	J21	με	Jauge de déformations submersible uniaxiale en ½ pont HBW-35-250-6-	≈±1000 με	N/A
22	Déformation de la tige A	J22	με	Jauge de déformations submersible uniaxiale en ½ pont HBW-35-250-6-	≈±1000 με	N/A
23	Déformation de la tige B	J23	με	Jauge de déformations submersible uniaxiale en ½ pont HBW-35-250-6-	≈±1000 με	N/A
24	Déformation de la bielle A8	J24	με	Jauge de déformations submersible uniaxiale en ½ pont HBW-35-250-6-	≈±1000 με	N/A
25	Déformation de la bielle A14	J25	με	Jauge de déformations submersible uniaxiale en ½ pont HBW-35-250-6-	≈±1000 με	N/A
26	Déformation de la bielle B8	J26	με	Jauge de déformations submersible uniaxiale en ½ pont HBW-35-250-6-	≈±1000 με	N/A
27	Déformation de la bielle B14	J27	με	Jauge de déformations submersible uniaxiale en ½ pont HBW-35-250-6-	≈±1000 με	N/A
28	Pression dans la galerie rive droite	P1	kPa	Capteur de pression différentielle (Intérieur-Extérieur) Druck 54-275-	5 psi	0.050%
29	Pression dans la galerie rive gauche	P2	kPa	Capteur de pression différentielle (Intérieur-Extérieur) Druck 54-275-	5 psi	0.050%
30	Pression d'air ou d'eau dans le reniflard	P3	kPa	Capteur de pression submersible Druck 54-276-68	10 psi	0.050%
31	Pression Pitot dans le reniflard	V3	kPa	Tube de Pitot avec capteur de pression différentielle Rosemount	-7 à 24 kpa	0.080%
32	Pression sur la vanne A position P4	P4	kPa	Capteur de pression absolue miniature PTX1830-3621268	70 psi	0.050%

Table A3 - Instrumentation list, instruments 33 to 55.

N° du signal	Nom du signal	Abréviation	Unité	Type de capteur	Plage	Pente
33	Pression sur la vanne A position P5	P5	kPa	Capteur de pression absolue miniature PTX1830-3621269	70 psi	0.050%
34	Pression sur la vanne A position P6	P6	kPa	Capteur de pression absolue miniature PTX1830-3644493	70 psi	0.050%
35	Pression sur la vanne A position P7	P7	kPa	Capteur de pression absolue miniature PTX1830-3644499	70 psi	0.050%
36	Pression sur la vanne A position P8	P8	kPa	Capteur de pression absolue miniature PTX1830-3469433	70 psi	0.050%
37	Pression sur la vanne B position P9	P9	kPa	Capteur de pression absolue miniature PTX1830-3469439	60 psi	0.050%
38	Pression sur la vanne B position P10	P10	kPa	Capteur de pression absolue miniature PTX1830-2937949	60 psi	0.050%
39	Pression sur la vanne B position P11	P11	kPa	Capteur de pression absolue miniature PTX1830-3644496	60 psi	0.050%
40	Pression sur la vanne B position P12	P12	kPa	Capteur de pression absolue miniature PTX1830-3469436	60 psi	0.050%
41	Pression sur la vanne B position P13	P13	kPa	Capteur de pression absolue miniature PTX1830-3644494	60 psi	0.050%
42	Pression sur la vanne B position P14	P14	kPa	Capteur de pression absolue miniature PTX1830-3930683	50 psi	0.050%
43	Pression sur la vanne B position P15	P15	kPa	Capteur de pression absolue miniature PTX1830-3907055	50 psi	0.050%
44	Course de la vanne A	CVA	mm	Traducteur de course Celesco 54-595-52	800 in	N/A
45	Course de la vanne B	CVB	mm	Traducteur de course Celesco 54-595-51	800 in	N/A
46	Pression entrée bâche	P bache	kPa	Capteur de pression Druck 54-277-83	100 psi	N/A
47	Synchronisation Compact RIO	Sync CRIO	V	Pulse 9V par batterie standard	0-9V	N/A
48	Proximètre moteur A	Prox A	mm	Proximètre Bently-Nevada 3300XL	11 mm	N/A
49	Proximètre moteur B	Prox B	mm	Proximètre Bently-Nevada 3300XL	11 mm	N/A
50	Vitesse de rotation du moteur	V moteur	rpm	Tachimètre optique avec multimètre HP-34411 (M-22-746-09 et M-16-734-11)	10 kHz	N/A
51	Perche A moulinet 1 (en bas)	M1	t/s	Moulinet SIAP 600582	8 m/s	N/A
52	Perche A moulinet 2	M2	t/s	Moulinet SIAP 600584	8 m/s	N/A
53	Perche A moulinet 3	M3	t/s	Moulinet SIAP 600586	8 m/s	N/A
54	Perche A moulinet 4	M4	t/s	Moulinet SIAP 600585	8 m/s	N/A
55	Perche A moulinet 5	M5	t/s	Moulinet SIAP 600587	8 m/s	N/A

Table A4 - Instrumentation list, instruments 56 to 73.

N° du signal	Nom du signal	Abréviation	Unité	Type de capteur	Plage	Pente
56	Perche A moulinet 6	M6	t/s	Moulinet SIAP 600591	8 m/s	N/A
57	Perche A moulinet 7	M7	t/s	Moulinet SIAP 600593	8 m/s	N/A
58	Perche A moulinet 8	M8	t/s	Moulinet SIAP 600594	8 m/s	N/A
59	Perche A moulinet 9 (en haut)	M9	t/s	Moulinet SIAP 600595	8 m/s	N/A
60	Perche B moulinet 1 (en bas)	M10	t/s	Moulinet SIAP 600535	8 m/s	N/A
#61	Perche B moulinet 2	M11	t/s	Moulinet SIAP 600536	8 m/s	N/A
62	Perche B moulinet 3	M12	t/s	Moulinet SIAP 600539	8 m/s	N/A
63	Perche B moulinet 4	M13	t/s	Moulinet SIAP 600541	8 m/s	N/A
64	Perche B moulinet 5	M14	t/s	Moulinet SIAP 600542	8 m/s	N/A
65	Perche B moulinet 6	M15	t/s	Moulinet SIAP 600544	8 m/s	N/A
66	Perche B moulinet 7	M16	t/s	Moulinet SIAP 600546	8 m/s	N/A
67	Perche B moulinet 8	M17	t/s	Moulinet SIAP 600578	8 m/s	N/A
68	Perche B moulinet 9 (en haut)	M18	t/s	Moulinet SIAP 600581	8 m/s	N/A
69	Tension au moteur	U moteur	V	Diviseur de tension résistif M-14-530-04	400 V	N/A
70	Courant au moteur B	I moteur B	A	Pince ampèremétrique Hioki M-19-195-02	100 A	N/A
71	Courant au moteur A	I moteur A	A	Pince ampèremétrique Hioki M-19-195-01	100 A	N/A
72	Puissance produite	Puissance	MW	Signal de la centrale	48 MW	N/A
73	Synchronisation LOGEC	Sync LOGEC	V	Pulse 9V par batterie standard	0-9V	N/A

Appendix C – A flow chart

of time stepping computation

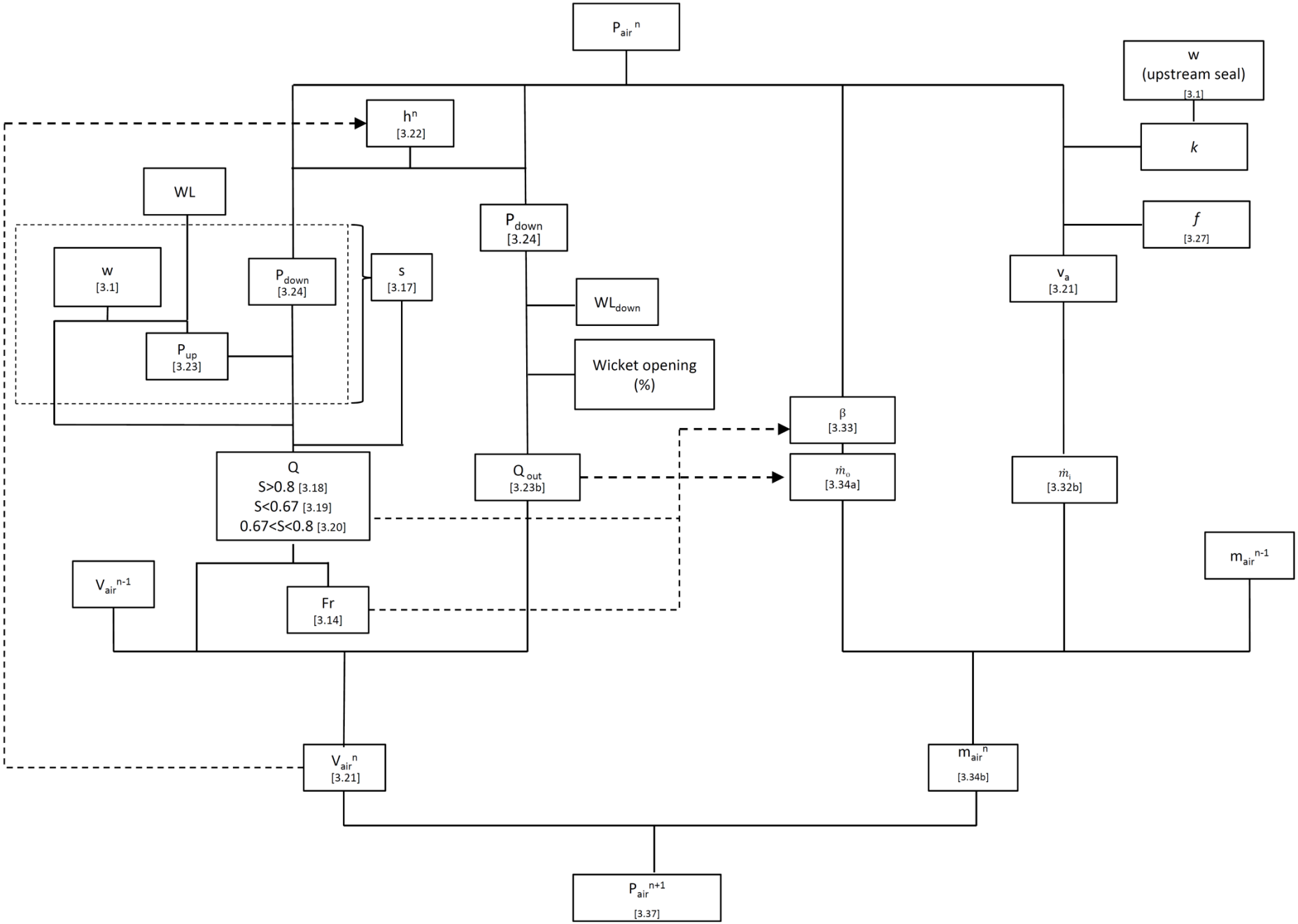
P_{air}^{n}
w (upstream seal) [3.1]
h^n [3.22]
k
WL
P_{down} [3.24]
f [3.27]
w [3.1]
P_{down} [3.24]
s [3.17]
v_a [3.21]
WL_{down}
P_{up} [3.23]
Wicket opening (%)
β [3.33]
Q
S>0.8 [3.18]
S<0.67 [3.19]
0.67<S<0.8 [3.20]
Q_{out} [3.23b]
$\dot{m}_o$ [3.34a]
$\dot{m}_i$ [3.32b]
m_{air}^{n-1}
V_{air}^{n-1}
Fr [3.14]
V_{air}^{n} [3.21]
m_{air}^{n} [3.34b]
P_{air}^{n+1} [3.37]